REPORT DOCUMENTATION PAGE		Form Approved OMB No. 0704-0188

Public reporting burden for this collection of information is estimated to average 1 hour per response, including the time for reviewing instructions, searching existing data sources, gathering and maintaining the data needed, and completing and reviewing this collection of information. Send comments regarding this burden estimate or any other aspect of this collection of information, including suggestions for reducing this burden to Department of Defense, Washington Headquarters Services, Directorate for Information Operations and Reports (0704-0188), 1215 Jefferson Davis Highway, Suite 1204, Arlington, VA 22202-4302. Respondents should be aware that notwithstanding any other provision of law, no person shall be subject to any penalty for failing to comply with a collection of information if it does not display a currently valid OMB control number. **PLEASE DO NOT RETURN YOUR FORM TO THE ABOVE ADDRESS.**

1. REPORT DATE (DD-MM-YYYY) 02 September 2015	2. REPORT TYPE Thesis	3. DATES COVERED (From - To) 12 August 2015 – 02 September 2015
4. TITLE AND SUBTITLE Fluid-Structure Interaction Effects on Mass Flow Rates in Solid Rocket Motors		**5a. CONTRACT NUMBER**
		5b. GRANT NUMBER
		5c. PROGRAM ELEMENT NUMBER
6. AUTHOR(S) William Harrigan		**5d. PROJECT NUMBER**
		5e. TASK NUMBER
		5f. WORK UNIT NUMBER Q0XZ
7. PERFORMING ORGANIZATION NAME(S) AND ADDRESS(ES) Air Force Research Laboratory (AFMC) AFRL/RQRM 4 Draco Drive Edwards AFB, CA 93524-7160		**8. PERFORMING ORGANIZATION REPORT NO.**
9. SPONSORING / MONITORING AGENCY NAME(S) AND ADDRESS(ES) Air Force Research Laboratory (AFMC) AFRL/RQR 5 Pollux Drive Edwards AFB, CA 93524-7048		**10. SPONSOR/MONITOR'S ACRONYM(S)**
		11. SPONSOR/MONITOR'S REPORT NUMBER(S) **AFRL-RQ-ED-TP-2015-320**

12. DISTRIBUTION / AVAILABILITY STATEMENT
Approved for public release; distribution unlimited

13. SUPPLEMENTARY NOTES
For Master's Project Defense; Cal Poly Pomona; 02 Sept 2015
PA Case Number: #15472; Clearance Date: 8/31/2015

14. ABSTRACT

Determination of mass flow rate in a solid rocket motor is critical in the design of a new motor due to its effect on the thrust produced. Fluid-structure interaction (FSI) effects between the combusting gases and propellant alter the motor chamber pressure and mass flow rate. To account for the FSI effects on mass flow rate in an expedited fashion, an automated method of coupling computational fluid dynamics (CFD) to finite element analysis (FEA) is explored. A propellant flap in a cross flow is analyzed. Comparisons are made between an analytical solution, a solely CFD solution, a manual FSI solution, and an automated FSI solution. The one-way FSI analysis, effectively the un-deformed CFD solution, over-predicted the pressures and mass flow rates. The FSI analyses with two-way coupling provided a more accurate assessment of solid rocket motor internal ballistics.

15. SUBJECT TERMS
N/A

16. SECURITY CLASSIFICATION OF:			17. LIMITATION OF ABSTRACT	18. NUMBER OF PAGES	19a. NAME OF RESPONSIBLE PERSON E. Weber
a. REPORT **Unclassified**	**b. ABSTRACT** **Unclassified**	**c. THIS PAGE** **Unclassified**	SAR	73	**19b. TELEPHONE NO** (include area code) N/A

Standard Form
298 (Rev. 8-98)
Prescribed by ANSI
Std. 239.18

FLUID-STRUCTURE INTERACTION EFFECTS ON MASS FLOW RATES

IN SOLID ROCKET MOTORS

A Project

Presented to the

Faculty of

California State Polytechnic University, Pomona

In Partial Fulfillment

Of the Requirements for the Degree

Master of Science

In

Engineering

By

William R. Harrigan

2015

SIGNATURE PAGE

PROJECT:	FLUID-STRUCTURE INTERACTION EFFECTS ON MASS FLOW RATES IN SOLID ROCKET MOTORS
AUTHOR:	William R. Harrigan
DATE SUBMITTED:	Summer 2015
	Engineering Department

Dr. Ahmadi   _____

Project Committee Chair

Professor and Chair

Aerospace Engineering Dept.

Dr. George Harting   _____

Technical Adviser

Motors Branch

Air Force Research Laboratory

ABSTRACT

Determination of mass flow rate in a solid rocket motor is critical in the design of a new motor due to its effect on the thrust produced. Fluid-structure interaction (FSI) effects between the combusting gases and propellant alter the motor chamber pressure and mass flow rate. To account for the FSI effects on mass flow rate in an expedited fashion, an automated method of coupling computational fluid dynamics (CFD) to finite element analysis (FEA) is explored. A propellant flap in a cross flow is analyzed. Comparisons are made between an analytical solution, a solely CFD solution, a manual FSI solution, and an automated FSI solution. The one-way FSI analysis, effectively the un-deformed CFD solution, over-predicted the pressures and mass flow rates. The FSI analyses with two-way coupling provided a more accurate assessment of solid rocket motor internal ballistics.

ACRONYM LIST

a   burn rate constant

A_b burn area of the propellant

A_e area of the nozzle exit

A_t area of the throat

c*   characteristic exhaust velocity

C_p specific heat

E   Young's modulus

F   force

g   gravity

k   turbulent kinetic energy

kg   kilogram

l_p length of propellant segment

m   meters

mm   millimeters

$\dot{m}$ mass flow rate

n burn rate exponent

omega   rate of dissipation of k

P   local static pressure

Pa   pascal

P_c chamber pressure

p_e pressure at the nozzle exit

P_i calculated chamber pressure

p_0 pressure in the free-stream

P_0 reference pressure

psi   pounds per square inch

psia   pounds per square inch (absolute)

r burn rate

r_b radius of the bore

r_c radius of the constriction

r_e radius of the nozzle exit

r_i propellant burn rate at pressure P_i

r_0 reference burn rate

r_t radius of the throat

s second

SST   shear stress transport

t_c thickness of the constriction

t_p thickness of propellant segment

V_e exhaust velocity

ρ_s density of the solid propellant

v Poisson's ratio

TABLE OF CONTENTS

LIST OF TABLES

LIST OF FIGURES

Chapter 1

INTRODUCTION

Statement of the Problem

A solid rocket motor typically consists of a combustion chamber which contains the propellant, an igniter, and a throat and nozzle assembly. The combustion chamber is comprised of a metal or composite case with insulation on the inside to protect it from the hot gases. The throat and nozzle are designed to accelerate the exhaust gases which provide the thrust.

During ignition of a solid rocket motor, gases from the igniter flow towards the nozzle and ignite the surface of the propellant. The surface of the propellant then begins to combust and contributes additional gases to the chamber. The motor quickly reaches an initial steady-state operation phase when all of the exposed propellant surfaces have been ignited. The propellant surface proceeds to burn back until the burning surface reaches the wall (usually insulation) and the motor extinguishes.

The geometry of the propellant surface is tailored to produce the desired thrust profile. Thicker web sections of propellant (the distance from the bore to the wall) will burn for longer periods of time, or a cylindrical section of propellant will produce increasing thrust over time as the propellant burns back and larger burning surface areas are exposed. Large motors may even be assembled in segments due to manufacturing limitations. These segments may introduce features that interrupt the flow of gases or cause pressure drops across the segments. These pressure drops have the effect of applying loads on the remaining, unburned propellant.

Composite propellant in a solid rocket motor is a heterogeneous mixture of powdered metal fuel, a crystalline oxidizer, and a polymeric binder. There is a non-linear relationship between the applied strain and the induced stress in composite propellant. The value for Young's modulus of propellant can vary and is dependent on factors such as strain rate and the temperature of the propellant[1]. The strain rate that propellant within a motor experiences during ignition is difficult to predict, yet it plays an important role

1

in determining the structural response of the propellant. Additionally, the deforming propellant alters the flow path of the gases which in turn varies the load being applied to the propellant.

The burn rate of solid propellant is pressure dependent. Pressure drops within the chamber and across features such as segment joints create unequal burn rates throughout the motor. These factors leave four main interrelated effects within a solid rocket motor:

   1) the effect of burn rate on the chamber pressure produced,

   2) the effect of chamber pressure on the burn rate of the propellant,

   3) the effect of structural deformations on pressure drops within the motor chamber, and

   4) the effect of pressure in the flow on the deformation of the propellant.

Accurate prediction of solid rocket motor chamber pressure is essential to ensure that the motor is able to complete its intended mission. Accurate chamber pressure prediction with the use of modeling and simulation tools allows for a reduction in the number of static fire tests and redesigns required. If the chamber pressure is predicted to be higher than it actually is, then the motor case will be excessively heavy since it would have been designed for a higher pressure. If the chamber pressure is under-predicted, then the motor will have unacceptably low safety margins. Either of these cases results in a non-optimal motor design.

During the design of a solid rocket motor, an iterative process can be used to optimize the performance of the motor. Motor chamber pressure can be determined with analytical mass conservation calculations, but these may not account for the pressure drops and structural deformations which can occur. Computational Fluid Dynamics (CFD) analysis can give better performance predictions but does not account for the structural deformations. A one-way fluid-structure interaction (FSI) analysis can give an approximation of the structural deformation, but it does not capture the effect that the deformations have on the pressures. Two-way FSI analysis can account for all of the effects of interest and may be manual or automated. A manual, two-way FSI analysis can be tedious and too cumbersome for use

2

during multiple design iterations while an automated, two-way FSI analysis can be convenient, but may present convergence challenges with large deformations. These analysis methods will be explored and compared.

Chapter 2

LITERATURE REVIEW

Rocket Motor Performance

Solid rocket motor propellant considered here is composed of a powdered metal fuel, a crystalline oxidizer, and a polymeric binder. The mechanical properties of the propellant mixture are determined by the binder combined with the effects of the solid particles. The result is a non-linear viscoelastic material which is time-history dependent meaning that the propellant can cumulate damage due to repeated stresses. These stresses can result in the oxidizer crystals becoming disconnected from the binder which leads to an effective softening of the propellant. During motor ignition, the high strain rate on the propellant causes the propellant to behave more brittle than during low strain rate testing[1].

The burn rate of solid propellant is pressure dependent and be calculated from the local static pressure along the propellant wall as

$$r = aP^n \qquad (1)$$

where P is the chamber pressure and a and n are burn rate constants which are determined through testing of a propellant[1]. From Equation 1, the mass flow rate (conversion of solid propellant into gas) can be calculated as

$$\dot{m} = \rho A_b r \qquad (2)$$

where ρ is the density of the solid propellant, A_b is the burning surface areas, and r is the burn rate of the propellant. Note that the burn rate is dependent on the local static pressure, so the mass flow rate is also a local value.

The characteristic exhaust velocity, c*, is a figure of merit of the propellant and of the combustion chamber design. It is also independent of nozzle expansion characteristics. The characteristic exhaust velocity is given by

$$c^* = \frac{PA_t}{\dot{m}} \qquad (3)$$

where P is the chamber pressure, A_t is the area of the throat, and $\dot{m}$ is the mass flow rate[1]. The chamber pressure can be determined by combining Equations 1, 2, and 3, and re-arranging, such that

$$P = \frac{c * \rho A_b a P^n}{A_t}$$

Moving the P^n term to the left and combining with the P term, we get

$$P^{1-n} = c * \rho a \left(\frac{A_b}{A_t} \right)$$

Solving for the chamber pressure,

$$P = \left(c * \rho a \left(\frac{A_b}{A_t} \right) \right)^{\frac{1}{1-n}}$$

The result is that the chamber pressure can be calculated as

$$P\left(\frac{lb}{in^2} \right) = \left[c * \left(\frac{in}{\sec} \right) \bullet \rho \left(\frac{lb}{in^3} \right) \bullet a \left(\frac{in}{\sec} \right) \bullet \frac{1}{g} \left(\frac{\sec^2}{in} \right) \bullet \left(\frac{A_b}{A_t} \right) \right]^{\frac{1}{1-n}} \quad (4)$$

where g = 386.4 in/sec^2, the units of A_b and A_t cancel out, and n is dimensionless. In metric units, the term for gravity would not be required.

The rocket thrust equation shows the relationship between mass flow rate, chamber pressure, and the resulting thrust produced by a rocket. As shown on the NASA website reference[2], the rocket thrust equation is given by

$$Thrust = F = \dot{m}V_e + (p_e - p_0)A_e \quad (5)$$

where $\dot{m}$ is the mass flow rate, V_e is the exhaust velocity, p_e is the pressure at the nozzle exit, p_0 is the free stream pressure, and A_e is the area of the nozzle exit. This equation shows that an accurate prediction of the mass flow rate is required to predict the thrust of a solid rocket motor.

Bore choking is one way in which a solid rocket motor may fail. It occurs when the unburned propellant is forced into and restricts the flow of gases within the combustion chamber. This restriction of the fluid

results in an increase in the head-end pressure which further moves the propellant. This runaway phenomenon can result in over-pressurization of the case or mechanical failure of the propellant. The cause has been shown to be propellant modulus that is below a critical value[3].

Computational Fluid Dynamics in Solid Rocket Motors

The computational fluid dynamics (CFD) code Fluent™ is frequently used in the flow analysis of solid rocket motors. The combustion gas is also commonly assumed to be of a single phase (gas) as opposed to the actual fluid which may contain burning aluminum in the liquid and solid phase. To account for this, the equivalent molecular weight of the gas is used. The fluid is assumed to be a homogeneous mixture of gas and particles, chemically frozen, and calorically perfect[4].

Structural Modeling of Solid Rocket Motor Propellant

The structural modeling of solid propellant can be accomplished with the finite element solver ABAQUS™. ABAQUS™ is able to utilize linear elastic models as well as various non-linear and viscoelastic models. The choice of model depends on the fidelity of the analysis desired (due to funding and time constraints), the fidelity of the tools available to the analyst, and the variety of test data available as input to the model.

The structural response of the propellant (i.e. its stiffness) is dependent on the rate at which pressure is applied[1]. During motor ignition a rapid pressurization occurs which quickly strains the propellant. If the fidelity of the structural analysis model is such that an elastic modulus is needed, then a high strain rate tensile test while under pressure will produce the needed model input data. Structural analysis for a solid rocket motor that is in storage conditions would require very low strain rate tests[5]. The difference in strain rate would be selected to replicate the loading condition on the propellant. In this way, the modulus value used would depend on the analysis that is being conducted. A number of methods have been employed to determine the correct modulus value to use for propellant undergoing ignition[3,4].

Fluid-Structure Interaction Modeling in Solid Rocket Motors

The fluid and structural events which occur within a solid rocket motor are coupled. Modeling and simulation frameworks have been developed with varying degrees of closeness of the coupling. Coupling methods have been characterized as being one-way or two-way. Additionally, two-way coupling may be

described as weak or strong[6]. One-way coupling involves the fluid model solution producing the pressure boundary condition on the structure, and then the structure deforms under the applied load. In two-way coupling, pressure from the fluid model is applied to the structure, and the structure deforms. The deformation of the structure is then applied to the fluid model.

In strong two-way coupling the fluid model in a transient simulation solves for the pressure values. These pressures are then applied to the structural model which is solved and deforms due to the pressure load. The displacements of nodes along the fluid-structure interface are interpolated to the fluid mesh. Multiple iterations of this inner loop are completed until changes in pressure and displacements are minimized and convergence is achieved.   For weak two-way coupling, multiple iterations are not calculated and the simulation moves to the next time step[6].

Two-way fluid-structure interactions can also be automated or manual. In an automated FSI, a computer handles the tasks of interpolating the pressures and displacements. Computer software would also handle the task of deforming the fluid mesh. Depending on the amount of deformation and the coefficients for mesh stiffness used, the automated FSI may result in a low quality fluid mesh in the deformed state[6].   According to Dr. Farhad Davoudzadeh, CFD analyst at the Air Force Research Laboratory, care should be taken in creating CFD meshes that will undergo deformation. The expected deformation should be accounted for when creating the mesh so that the deformation does not adversely skew the elements. In manual FSI, more time is spent in interpolating the pressures and displacement, but more control is provided to the analyst in creating the fluid mesh for the deformed geometry.

Chapter 3

METHODOLOGY

Motor Definition

The solid rocket motor designed in this work exaggerates the effects of fluid-structure interactions and could possibly be used for a future validation effort. An axisymmetric design, shown in Figure 1, was selected for simplicity and is applicable to many solid rocket motor designs.
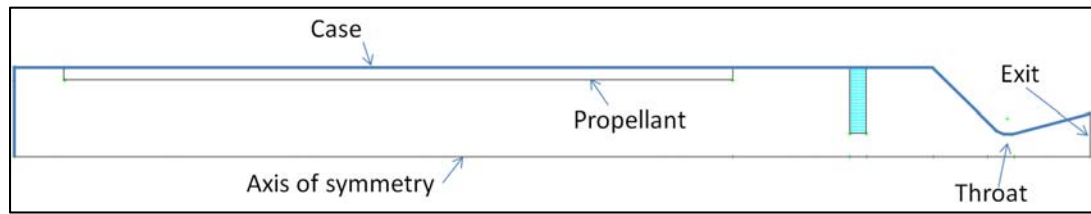

Figure 1: Motor components

The motor has two grains, labelled A and B in Figure 2. Grain A is in the head-end of the motor and is made from propellant. Grain A produces the mass flow into the motor. Grain B is used as a constriction to the flow and is made from a non-burning material but with the same mechanical properties as propellant. Grain B was designed to maximize the deformation effect. The throat of the motor is shown with its radius dimension r_t. Gases from grain A flow past the constriction caused by grain B and exit the motor on the right side of Figure 2.
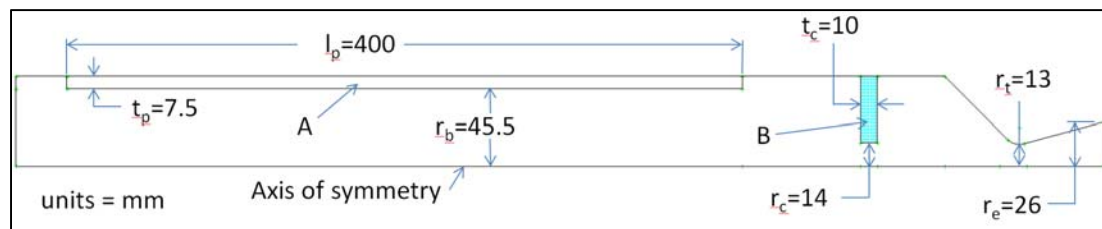

Figure 2: Motor Dimensions and Propellant Segments

The fluid volume of the motor can be broken down into two main regions, as shown in Figure 3. Pressure is measured in both the head-end and aft-end. Grain B creates a pressure drop across it due to its constriction of the flow. This pressure drop can be measured as the difference between the head-end and aft-end pressures. Figure 3 shows the pressure measurement locations as lines. The average of all pressure values along the line indicated is taken as the measured value. The burn rate used in the CFD

8

solution is based on the local pressure along the propellant surface and not on the calculated head-end pressure.
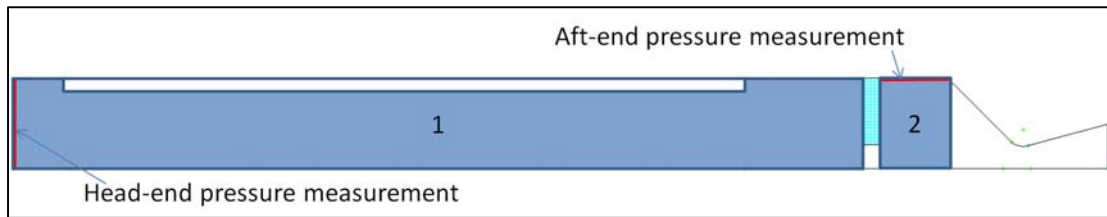

Figure 3: Motor Regions

Table 1 shows the properties used in the analysis.

Table 1: Fluid and Structure Model Input Values

Propellant	Burn Rate Pressure Exponent, n	.34 (unitless)
	Reference Burn Rate, r_0	7.0 mm/s @ 6.89 MPa
	Young's Modulus, E	55.2 MPa
	Poisson's Ratio, v	0.499 (unitless)
	Density, ρ_s	1802 kg/m^3
Gas Properties	Gas Temperature	3,500 K
	Molecular Weight	29.56 kg/kmole
	Specific Heat, C_p	4113 J/K•kg
	Viscosity	1.034E-4 mP
	Characteristic Exhaust Velocity, c*	1,576 m/s

<u>Analytical Solution</u>

Utilizing the geometry and dimensions provided in Figure 2, and considering that the motor is axisymmetric, the burn surface area and the throat areas can be determined. Shown in Figure 4, the burn area is determined from the addition of the inner bore area and the area of the two sides of grain A.
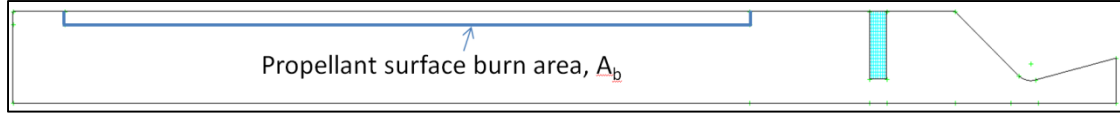
Approved for public release; distribution is unlimited. PA#

Propellant surface burn area, A_b

Figure 4: Propellant burn area

The areas of the throat and burn surface are shown in Table 2.

Table 2: Burn and Throat Areas

Burn Surface Area, A_b	118,996 mm^2
Throat Area, A_t	531 mm^2

Utilizing Equation 4 and the values found in Tables 1 & 2, the chamber pressure is calculated to be 3.55 MPa (515 psia). The predicted chamber pressure can then be used to determine the mass flow rate by first calculating the propellant burn rate at the expected chamber pressure. This accomplished by considering Equation 1 for both the reference condition (pressure and burn rate) and at the calculated pressure. At the reference condition, the burn rate is given by

$$r_0 = aP_0^n \tag{6}$$

with the values shown in Table 1. At the calculated chamber pressure (P_i), with a and n held constant, the burn rate is given by

$$r_i = aP_i^n \tag{7}$$

where P_i has been determined with Equation 4. Dividing Equation 7 by Equation 6 and solving for r_i, one gets

$$r_i = r_0 \left(\frac{P_i}{P_0}\right)^n \tag{8}$$

where the burn rate at the calculated chamber pressure is found to be 5.59 mm/s. Utilizing Equation 2 while considering the entire burning surface area as shown in Table 2, the mass flow rate associated with the calculated chamber pressure and burn rate is given by

$$\dot{m} = \rho_s A_b r_i \tag{9}$$

From Equation 9, the mass flow rate at the calculated chamber pressure is 1.198 kg/s.

Computational Fluid Dynamics Solution

Utilizing the computational fluid dynamics code ANSYS Fluent™ version 14.5, the same motor was analyzed. In this case, a user defined function (UDF) is utilized to simulate the pressure dependent burn rate along the propellant surface. The static pressure calculated by the CFD solution is compared to the reference pressure, the pressure at which the burn rate was measured, and the burn rate is then given by Equation 8. This process is completed for each element along the entire propellant surface. The appropriate mass is inserted into the solution space according to Equation 9 by considering the density of the propellant and the area covered by the element. The temperature of the inlet mass flow is equal to the flame temperature of the burning propellant as determined by experiment. In this case, the inlet temperature is a constant 3,500 K. Since one-way FSI coupling does not update the fluid mesh due to structural deformations, the results of this CFD solution represent the mass flow predictions of the one-way FSI coupling.

A computational fluid dynamics mesh was created for the fluid region of the motor. The mesh, shown in Figure 5, has various boundary conditions specified for each of the zones. The mass flow inlet is controlled by the user defined function described above. The pressure outlet is set to sea-level pressure conditions (101,325 Pa). The axis of symmetry is used so the solution can replicate an entire 360° rotation. Adiabatic walls are used for the rest of the boundary conditions.
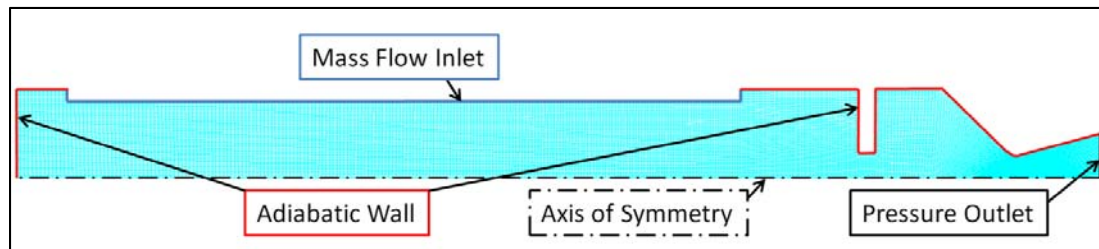

Figure 5: CFD Mesh and Boundary Condition Zones

The gas properties from Table 1 were used for the fluid. The pressure-based solver was used, and the viscous model was set to k-omega SST. The UDF that converts pressure to mass inlet flow needs an initial condition to begin, so 20 iterations were calculated using the specified inlet mass flow rate of 1.2 kg/s.

After that, the user defined function was used to determine the mass inlet flow. Residuals were monitored, but the value of the residuals was not used as a convergence criteria. The solution was allowed to proceed until the residuals appeared to no longer decrease. The mass flow rate at the propellant inlet was compared to the mass flow rate at the nozzle exit to ensure mass conservation. In this case, the mass conservation error was shown to be less than 2E-7%.

Manual Fluid-Structure Interaction Solution

As shown in the pressure contours in Figure 11, grain B can produce a large pressure drop due to the restriction it creates in the flow. The pressure drop across grain B would create an unbalanced pressure load on the segment. Additionally, shear stresses would produce a load on the grain, but that force is ignored in these calculations. This pressure load could cause a deformation of grain B due to the relatively low modulus of the material. As the material deforms the results from the CFD solution would change. New pressures would create new burn rates, and a new equilibrium condition would exist. The manual FSI solution was the first of 2 two-way FSI coupling analyses.

A method of accounting for this fluid-structure interaction effect is to utilize the results of the CFD solution and then apply the resulting pressure values to a structural model. Figure 6 shows the pressures that are applied to grain B. A check was conducted to ensure that the pressures produced in the CFD solution matched the boundary condition loads applied to the structure. Each element along the surface of the finite element model obtains a pressure value from the CFD element nearest to its midpoint. The color and length of the arrows representing the pressure boundary condition on the structure in Figure 6 are indicative of the magnitude of the pressure. For instance, the maximum pressure on the windward side of Grain B is 4.35 MPa (631 psi), and the minimum pressure on the leeward side of Grain B is 2.61 MPa (378 psi).
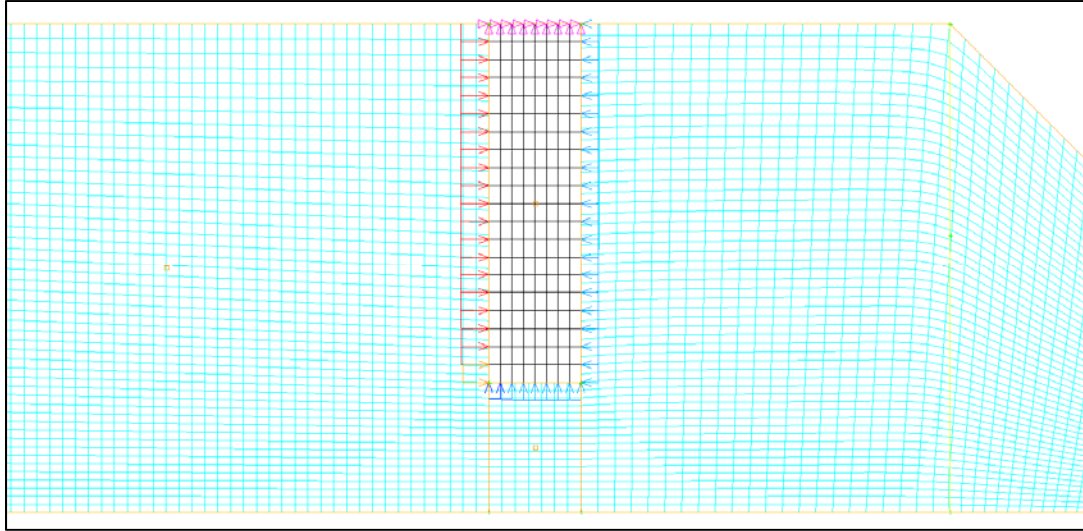
A finite element analysis was then conducted on the structural model utilizing the commercially available code ABAQUS™ version 6.14. A static analysis was used to determine the deformation of grain B. The propellant in grain A was not expected to undergo significant deformation, so pressure loads were not applied to it. A value for Young's modulus was taken from the tri-axial, high strain rate test data presented in a propellant aging study[5]. Though the propellant used in this experiment is different, the value is a reasonable approximation. Figure 7 shows the resulting deformed structure (black mesh), the un-deformed fluid mesh, the applied pressure loads, and the spatially fixed position boundary conditions (pink triangles) on the model. The default convergence criterion was used in ABAQUS™ version 6.14, specifically that the ratio of the largest residual to the corresponding average flux norm value was set to 5E-3. In this case, the flux is the value being monitored (i.e. force and moment)[7].
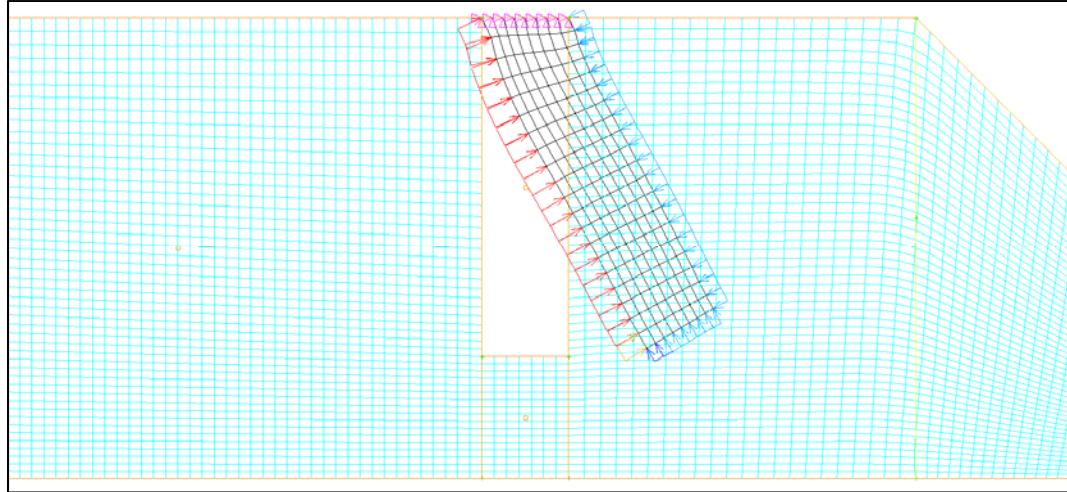
Figure 7: Deformed Structure due to Applied Pressure Loads

Utilizing the deformed structure from Figure 7, a new CFD mesh was created. First, the outline of the deformed structure was traced. A fluid mesh was then created to fill the fluid region. The number of elements used in the deformed fluid mesh was the same as in the initial CFD mesh. This was done to allow for comparison with the automated FSI solution since that solution retains the same number of elements throughout the solution. Figure 8 shows the deformed fluid mesh (blue) along with the deformed structure that was used to define the deformation.
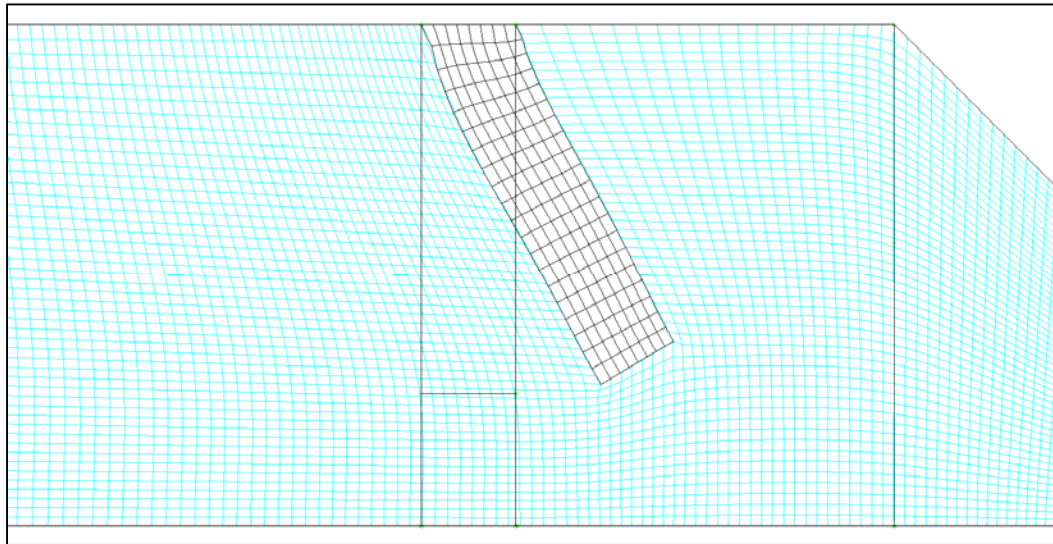

Figure 8: Deformed Fluid Mesh, Manual FSI Method

The deformed fluid mesh was then set up to be solved with ANSYS Fluent™. The same gas properties and mass flow inlet boundary conditions as before were used, including the user defined function which

Approved for public release; distribution is unlimited. PA#

captures the pressure dependent mass inlet flow amounts. The solution was allowed to proceed until the residual values appeared to no longer decrease, and negligible mass conservation error was shown between the propellant inlet and the nozzle exit. In this case, the mass conservation error was shown to be less than 9E-14%.

<u>Automated Fluid-Structure Interaction Solution</u>

An automated fluid-structure interaction analysis was conducted to generate a multiple iteration solution. A software program called FEM Builder™ was used to complete the automated fluid-structure interaction analysis. A description of the software can be found in Isaac and Iverson[8]. The solution was controlled by a script written in the programming language Python. The solution begins with the initial CFD model being solved with ANSYS Fluent™. The calculated pressures are then automatically applied to a structural model. An input file for ABAQUS™ is then generated and executed. The resulting deformations are then applied to the fluid model. The CFD model, with a mesh that matches the deformed structure, is solved with ANSYS Fluent™. This process is repeated until the predefined convergence criteria are met. The maximum static pressure and maximum displacement were recorded after each solution was complete. When the difference in both of these values fell below 0.1% between subsequent iterations the solution was considered converged. The automated FSI solution is similar to the strongly coupled two-way FSI except that the analysis here is not transient. Steady-state fluid and static structural analyses are conducted.

A challenge with the automated fluid-structure interaction analysis was the automated deformation of the fluid mesh. Deformation of the structural mesh occurs within ABAQUS™ during the FEA solution. The fluid mesh is stretched from its original shape to the deformed shape. During the first iteration, the amount of deformation can be quite large and result in a "twisted", or unsolvable, CFD mesh. To overcome this challenge, the magnitude of the pressure boundary condition applied to the structure during the first 5 iterations was reduced by a factor. This loading factor allowed for the pressure load to be ramped up over the first 5 iterations, thereby preventing extreme deformation and solution failure.

Approved for public release; distribution is unlimited. PA#

During the 5th and subsequent iterations, the full amount of pressure calculated in the CFD solution was applied to the structure as the loading boundary condition.

The fluid and structural models contained the same properties as the manual fluid-structure interaction solution. A plot of the resulting maximum static pressure and deformation is shown in Figure 9. The ramp up of the pressure load on the structure is evidenced by the gradual increase in displacement amounts, both axially and radially. The ramp up of pressure prevents an "overshoot" of the displacement when failure due to excessive deformation is likely. As the displacement amounts increase, the pressure decreases. The pressure and displacements then appear to even out, and the convergence criteria of < 0.1% change are met after 14 iterations.
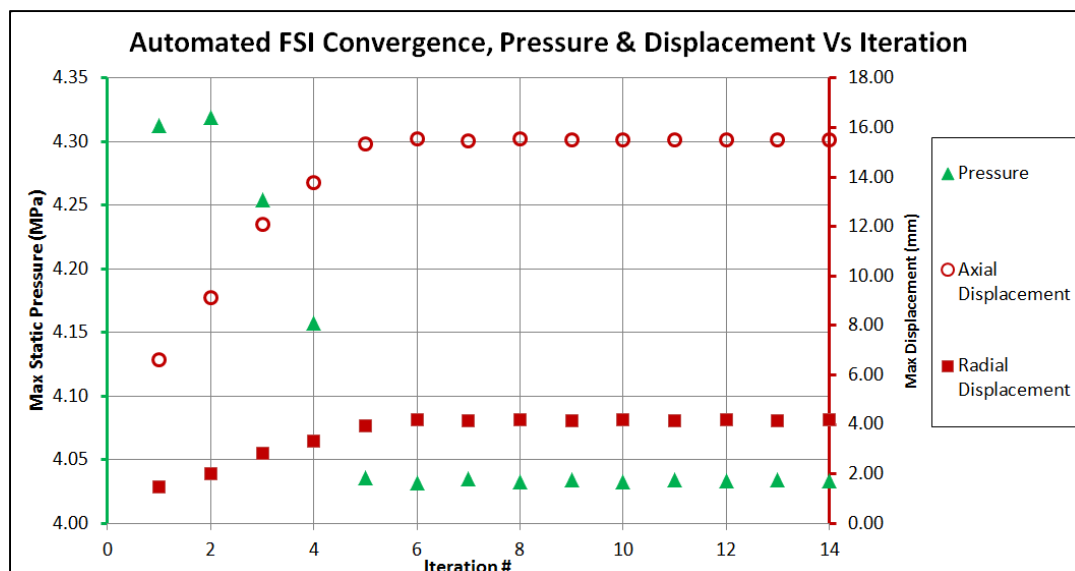

Figure 9: Automated FSI Convergence Monitoring

Of note in Figure 9 is that the values being monitored for FSI convergence appear to level off after iteration number 6, yet convergence is not achieved until iteration number 14. Part of this is due to the convergence criteria being set to 0.1% change in value. For the pressures being monitored, this translates to a change of less than ~620 Pa. For the displacement amounts which occurred, a 0.1% change is equivalent to ~ 0.01 mm. Both of these convergence criteria need to be met during the same iteration, so

Approved for public release; distribution is unlimited. PA#

small oscillatory behaviors would tend to delay convergence. The mass conservation error for the automated FSI analysis was shown to be approximately 7E-5%.

Chapter 4

RESEARCH FINDINGS

The un-deformed CFD solution converged and produced an estimate of the head end pressure and mass flow rate. Figure 10 shows a plot of the residuals and the calculated mass flow rate for the inlet (propellant) and for the exit. The values of the residuals are on the order of 10e-5 to 10e-13 and are no longer changing.
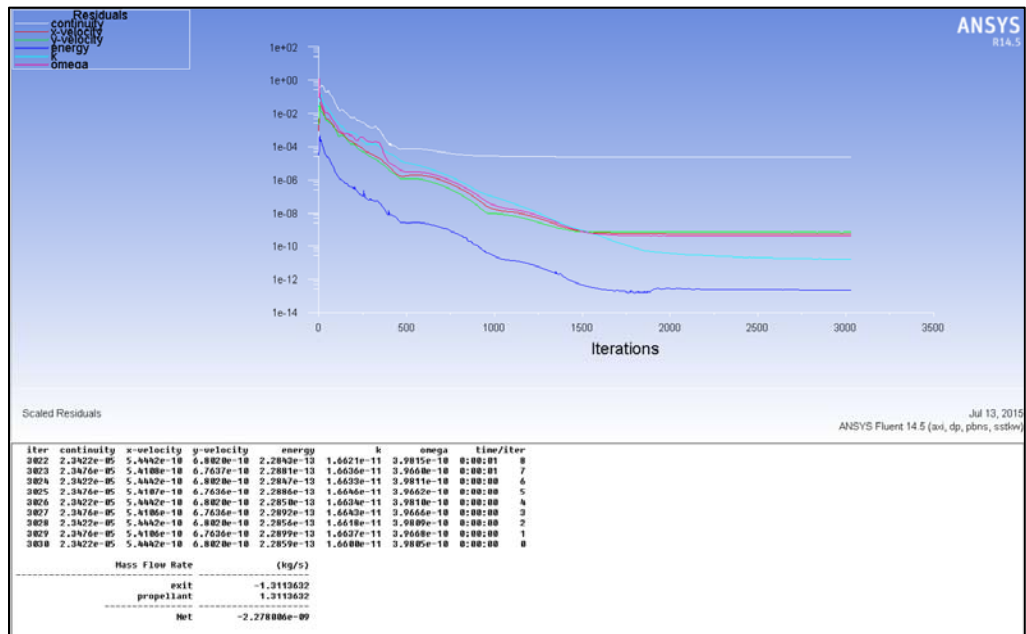

Figure 10: CFD Solution, Residuals and Mass Flow Rate

The CFD solution was also used to determine the expected head-end chamber pressure (Section 1 in Figure 3). The pressure in the head-end section appears fairly uniform across the propellant surface. Contours of the static pressure are shown in Figure 11. The head-end pressure was found to be 4.35 MPa and the mass flow rate was found to be 1.31 kg/s. A large pressure drop can be seen across grain B.
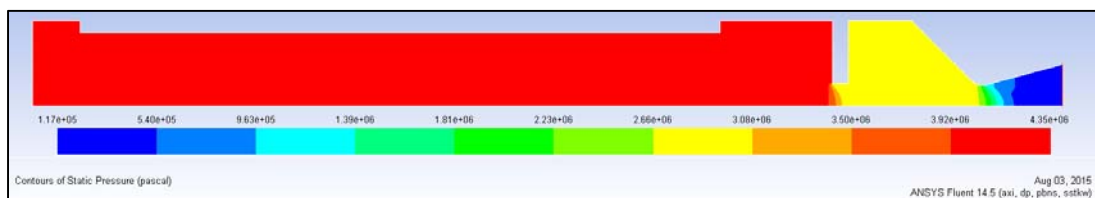

Figure 11: CFD Solution, Static Pressure Contours

Approved for public release; distribution is unlimited. PA#

The CFD residuals for the manual FSI method are shown in Figure 12. The residual values obtained are on the order of 1e-10 to 1e-15 and are no longer changing. The FEA convergence criterion used is specified in the manual FSI analysis section above.
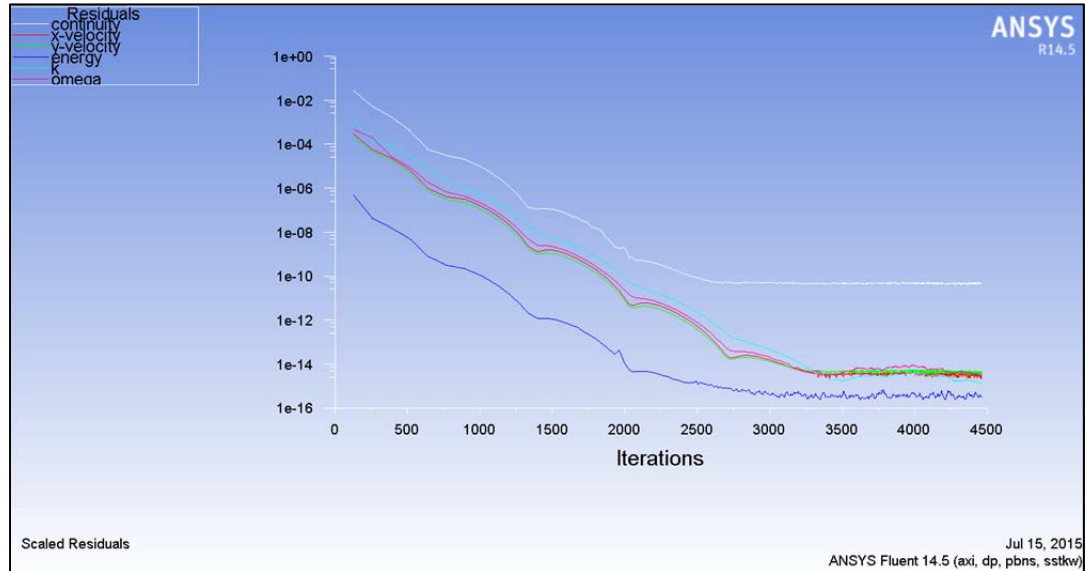

Figure 12: Residuals of Deformed CFD, Manual FSI Method

Pressure contours and the mass flow rate were then calculated by ANSYS Fluent™. Figure 13 shows a contour plot of the static pressure and a print out of the mass flow rate. Similar to before, negligible mass conservation error is calculated between the propellant inlet and the nozzle (exit). Head end pressure was shown to be 3.92 MPa and the mass flow rate was 1.25 kg/sec.

Figure 13: Static Pressure and Mass Flow Rate, Deformed CFD model, Manual FSI Method

Additional iterations of the manual FSI could have been conducted to account for the change in head end pressure which occurs due to the deformation of the aft segment. The single iteration of the manual

Approved for public release; distribution is unlimited. PA#

fluid-structure interaction method was conducted to gauge the amount of time needed to conduct such an analysis. An automated FSI method would be needed if additional iterations were desired.

The automated FSI approach was used to conduct multiple fluid-structure interaction iterations. The static pressure contours are shown in Figure 14. The mass flow rate, as calculated by ANSYS Fluent™ at the propellant inlet and nozzle exit, is printed in the figure as well. Negligible mass conservation error is shown in the solution.
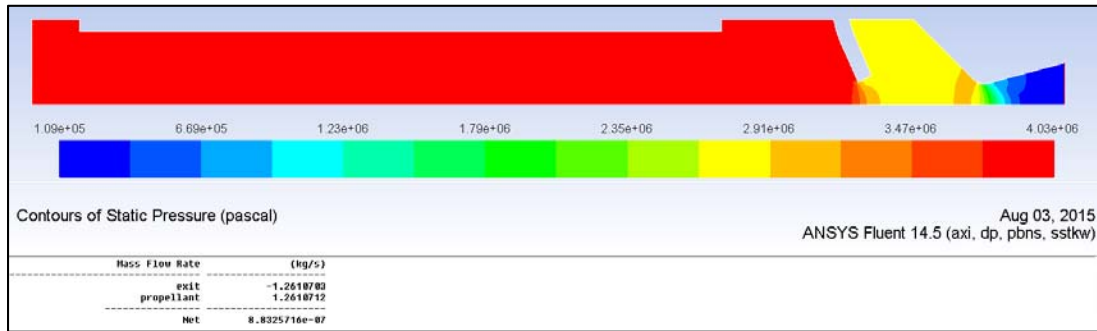

Figure 14: Static Pressure Contours, Automated FSI Solution

The residuals for the CFD solution are shown in Figure 15. These values do not drop as dramatically as the previous, non-automated solution. An examination of the deformed CFD meshes was conducted to determine the cause of the large residual values.
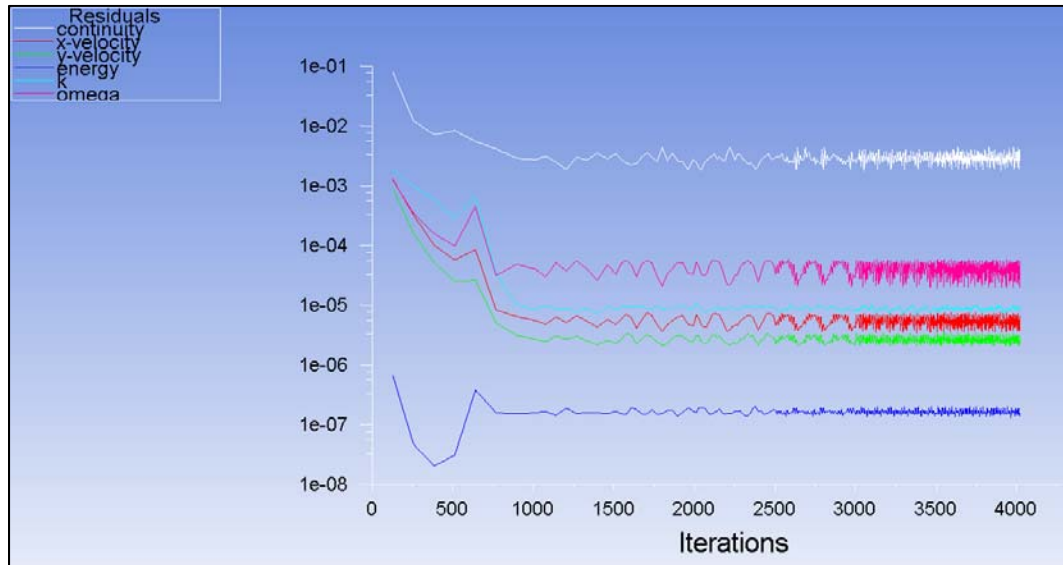

Figure 15: Residuals, Automated FSI Solution, Iteration # 14

Approved for public release; distribution is unlimited. PA#

As can be seen in Figure 16, the region around the trailing (right) tip of the deforming segment contains highly skewed CFD elements. This is due to the large deformation created with this geometry. Skewed elements such as this may be caused by the mesh stiffness coefficients used in the deformation of the fluid mesh[6]. In this case, however, the fluid mesh was deformed by a structural FEA solver. The skewed elements are the result of the surface buckling of the "structure" under the applied displacement of the boundary nodes. The skewed elements prevent a well converged solution, so the actual pressure may differ slightly from the pressures shown in Figure 14. These results highlight the need for ramping up the interpolated pressure boundary conditions onto the structural model. Without the ramp up for the pressure load, the structural deformation overshoots the final deformation. The deformation on the fluid mesh for the overshoot case is so severe that the CFD solution fails right away.
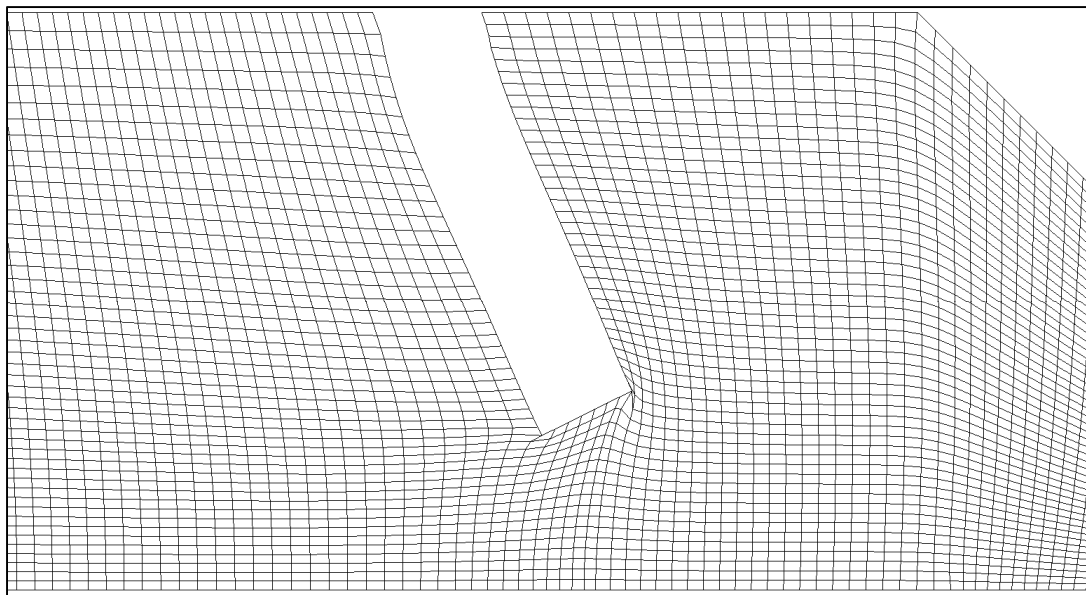

Figure 16: CFD Mesh Deformation, Automated FSI, Iteration # 14

Figure 17 is a comparison of results for head end pressure and mass flow rate from the four methods used. Additionally, the mass flow rate is shown as calculated by Fluent™ and as calculated from Equation 9 using the head end pressure determined by Fluent™. The relationship between mass flow rate and head end pressure is clearly visible, but up to a 2.2% difference exists between the two mass flow rate calculations. The cause of this difference is unknown. The pressure along the propellant surface, which determines the mass flow inlet amount, does not differ from the measured head-end pressure by enough

21

to account for this difference. The lowest head-end pressure is predicted by the analytical solution. The

initial CFD solution predicts the highest head-end pressure since the deforming structure is not accounted

for. The manual FSI solution, with its single iteration, predicts the second lowest head-end pressure.

After 14 iterations, the automated FSI solution predicts the head-end pressure to lie between the initial

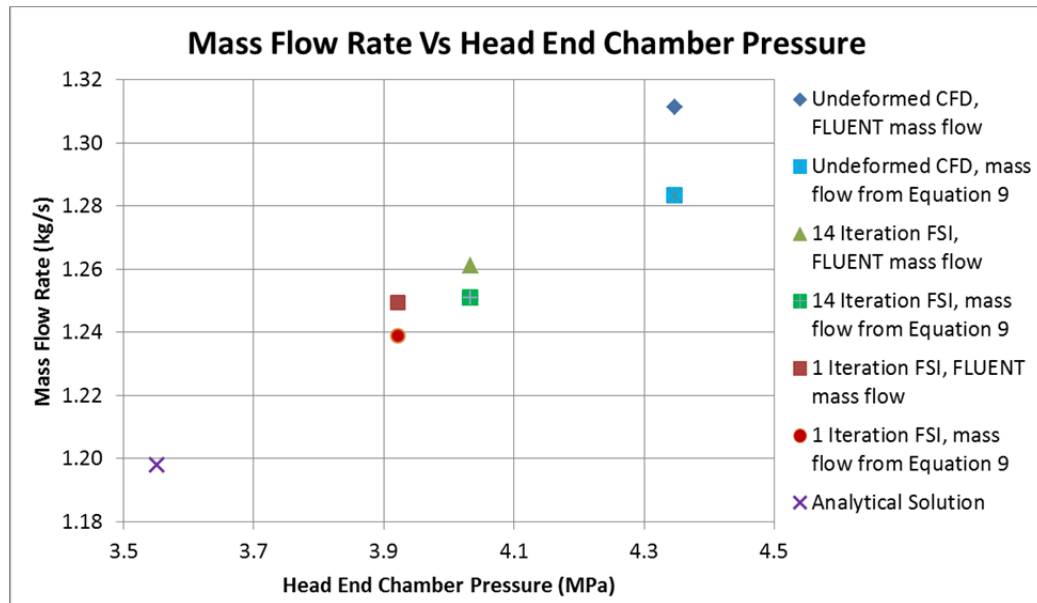CFD solution and the single iteration solution of the manual method.

Figure 17: Comparison of Mass Flow Rates and Head End Pressures

The initial geometry of the aft segment is shown in Figure 18 along with the final deformed geometries

from the manual and automated FSI solutions. Similar to the predicted head-end pressures, the resulting

geometry for the automated FSI solution lies between the initial geometry used in the CFD solution and

the single-iteration manual FSI solution. The large deformation seen in the manual FSI solution is due to

the fact that the pressure used to create the deformation is the large value from the initial CFD solution.

Additional FSI iterations allow for the effect of the structural deformation to be realized within the CFD

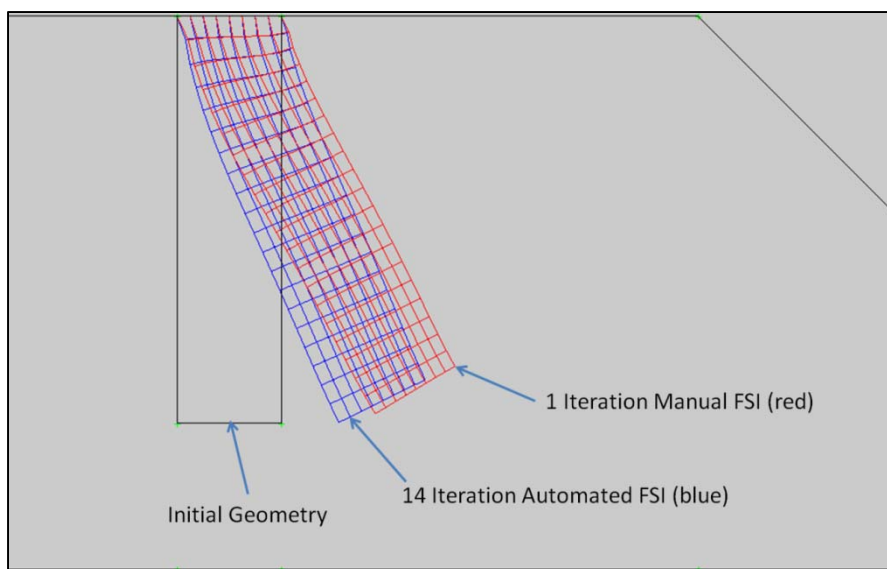solution. As the structure deforms, the head-end pressure drops.

Figure 18: Initial Geometry and FSI Deformed Geometries

Approved for public release; distribution is unlimited. PA#

Chapter 5

CONCLUSION

Accurate prediction of the pressure within a solid rocket motor is critical to ensure maximum performance while maintaining adequate margins of safety. An under-prediction of chamber pressure will result in a design with an unacceptably low margin of safety because the motor case will be designed for a lower pressure that it actually contains. Over-prediction of the chamber pressure will result in motor case that is heavier than necessary thereby decreasing motor performance. The optimal prediction of chamber pressure within a solid rocket motor needs to account for the structural deformations that occur in the propellant due to the pressure loads. In order to be useful during design iterations of a new motor, an automated fluid-structure interaction analysis tool is the best approach to determine motor pressure.

The analytical solution proved useful in quickly determining some approximate values related to motor geometry. Sizing of the throat area and burn surface areas to produce the desired chamber pressure were conducted using the analytical solution method. This method also provided results which could be used to determine the reasonableness CFD results.

The CFD method accounted for the pressure drop across the aft segment but did not account for the deformation of the segment. Due to not accounting for the deformation, the pressure drop was over predicted. The CFD solution was a challenge to setup, but once established, it could also be used in the FSI analyses.

The manual FSI method accounted for the pressure drop across the aft segment and accounted for the deformation of the segment. However, since the initial CFD solution over-predicted the pressure drop, the deformation was also over predicted. This resulted in the manual FSI solution, using the over-deformed geometry, predicting a lower chamber pressure and mass flow rate. Additional iterations would likely produce results similar to the automated FSI method, but the time to conduct such an analysis would be prohibitively long.

24

The automated FSI method accounted for the pressure drop across the aft segment as well as the change in pressure drop due to the deformation of the segment. The automated FSI method was able to utilize the initial CFD solution, so creation of an additional CFD mesh was not necessary.

The two-way coupling appeared to give more accurate results than the one-way coupling. As seen in Figure 18 the one-way coupling resulted in the 1 iteration manual FSI deformation. The one-way coupling over-predicts the deformation, while the two-way coupling provides a more accurate assessment of solid rocket motor internal ballistics.

REFERENCES

1   Sutton, George P. "Rocket Propulsion Elements" Fourth Edition, John Wiley & Sons, New

        York, 1976

2   NASA website https://www.grc.nasa.gov/www/K-12/airplane/rockth.html accessed 21 July

        2015

3   Murdock, John W.; Johnston, William A. "Flow-Structural Interaction in Solid Rocket Motors"

        NATO RTO-EN-023, Belgium, 2002

4   Rex, Brian W.; Wang, Qunzhen; Isaac, Daron, "An Automated Fluid-Structural Interaction

        Analysis of a Large Segmented Solid Rocket Motor", AIAA-2003-4507, 39th

        AIAA/ASME/SAE/ASEE Joint Propulsion Conference & Exhibit, July 20-23, 2003, Huntsville, AL

5   Manpa Report NR 473 (82), Propellant Surveillance Report ANB-3066 Propellant, Propellant

        Analysis Laboratory, Hill Air Force Base, UT, August 1982

6   Benra, Friedrich-Karl; Dohmen, Hans Josef; Pei, Ji; et.al. "A Comparison of One-Way and

        Two-Way Coupling Methods for Numerical Analysis of Fluid-Structure Interactions," Journal

        of Applied Mathematics, Volume 2011, Article ID 853560, 2011

7   Abaqus Version 6.14 Analysis User's Manual, Volume II, Part III

8   Isaac, Daron; Iverson, Michael, "Automated Fluid-Structure Interaction Analysis",

        ADA416478 Technical Reports www.dtic.mil accessed 15 July, 2015

Air Force Research Laboratory

Fluid-Structure Interaction Effects on Mass Flow Rates in Solid Rocket Motors, Master's Degree Project

Summer 2015

William Harrigan
AFRL/RQRM

Integrity ★ Service ★ Excellence

Agenda

- **Committee Members**
- **Solid Rocket Motor Overview**
- **Statement of the problem**
- **Methodology**
- **Research Findings**
- **Conclusion**
- **References**

Committee Members

- ## Dr. Ali Ahmadi

  Project Committee Chair

  Professor and Chair

  Aerospace Engineering Department

  California State University Pomona

- ## Dr. George Harting

  Technical Advisor

  Motors Branch

  Air Force Research Laboratory

Solid Rocket Motor Overview

- **Not a normal design, but shows components**
- **Case: may be steel, titanium, or composite[1]**
- **Propellant: bonded to case, polymer binder with powdered aluminum and crystalline ammonium perchlorate[1]**
- **Propellant flap (blue) is similar to residual inhibitor on forward face of an aft grain**
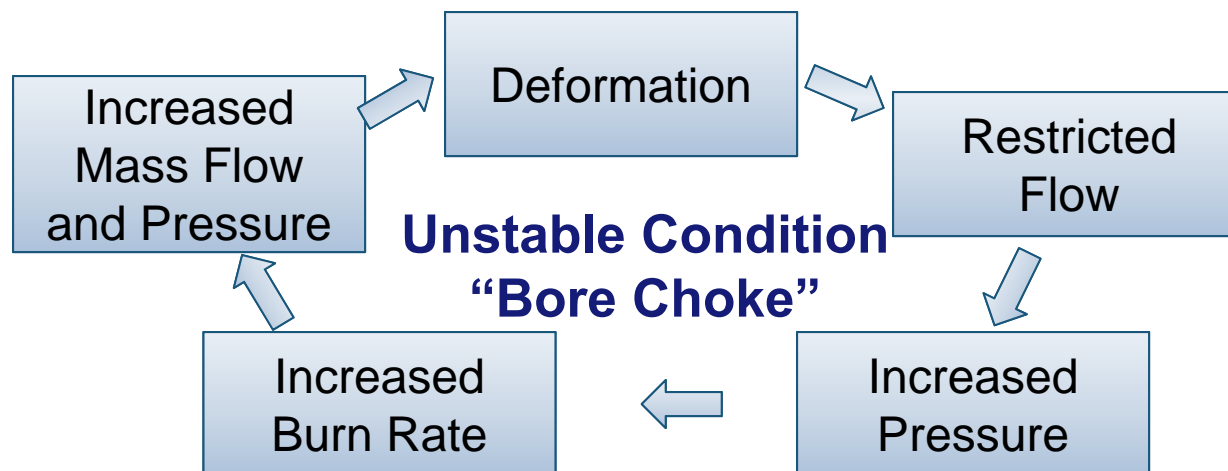

Case

Propellant

Axis of symmetry

Exit

Throat

AFRL
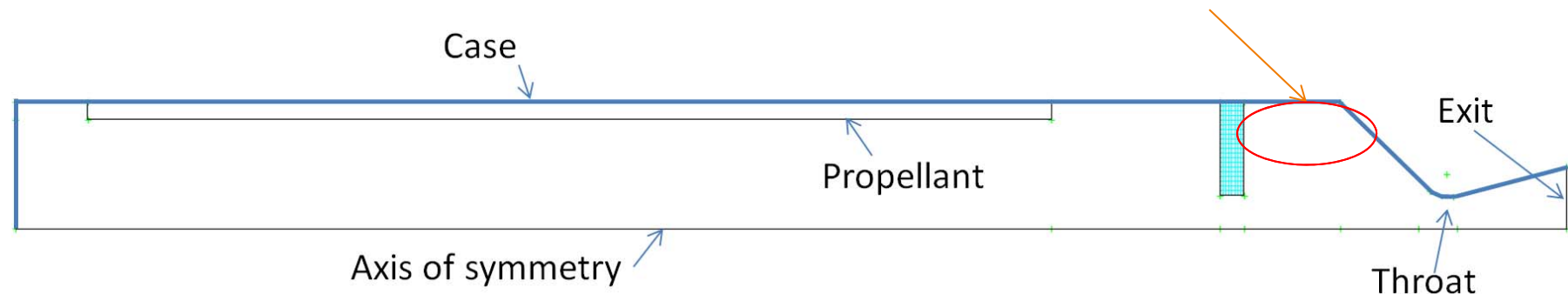
Statement of the Problem

- **Solid propellant can deform due to chamber pressure**

- **Deformation may restrict or aid flow**
  - **Alters chamber pressure due to pressure drops**

- **May be stable or unstable**
  - **Stability determined by <u>rigidity of propellant</u>[3]**

Approved for public release; distribution is unlimited. PA#

5

Rocket Motor Requirements

- ## Rocket motor design to meet requirements
  - ### Range
  - ### Payload
- ## Sub-requirements
  - ### Maximize thrust
  - ### Minimize weight
- ## Design requirements
  - ### Chamber pressure
    - Weight of case
    - Effect on mass flow rate $\rightarrow$ Thrust
  - ### Mass flow rate
    - Effect on chamber pressure $\rightarrow$ Thrust

Rocket Thrust Equation

- **Mass flow rate and chamber pressure affect thrust[2]**

$$Thrust = \dot{m}V_e + (P_e - P_0)A_e$$

$\dot{m}$ = mass flow rate

V_e = exhaust velocity at exit

P_e = pressure at exit

P_0 = freestream pressure

A_e = area of nozzle exit

Propellant Burn Rate

- **Solid rocket motor propellant burn rate is pressure sensitive[1]**

$$r = aP^n$$

r = burn rate

a = burn rate constant

P = pressure

n = burn rate exponent

- ***a* and *n* are determined experimentally[1]**

Mass Flow Rate

- ## Mass flow rate
  - ### Solid propellant → combustion gases

$$\dot{m} = \rho A_b r$$

$\dot{m}$ = mass flow rate

ρ = density of solid propellant

A_b = area of burning propellant

r = burn rate

Characteristic Exhaust Velocity

- **Depends on propellant and combustion chamber design[1]**

- **Independent of nozzle expansion characteristics[1]**

$$c^* = \frac{PA_t}{\dot{m}}$$

$c^* =$ characteristic exhaust velocity

$P =$ chamber pressure

$A_t =$ throat area

$\dot{m} =$ mass flow rate

Chamber Pressure

- **Combine and rearrange the 3 previous equations**

$$c^* = \frac{PA_t}{\dot{m}}$$

$$r = aP^n$$

$$\dot{m} = \rho A_b r$$

$$P\left(\frac{lb}{in^2}\right) = \left[c*\left(\frac{in}{sec}\right) \bullet \rho\left(\frac{lb}{in^3}\right) \bullet a\left(\frac{in}{sec}\right) \bullet \frac{1}{g}\left(\frac{sec^2}{in}\right) \bullet \left(\frac{A_b}{A_t}\right)\right]^{\frac{1}{1-n}}$$

- **Shown in English units**

Approved for public release; distribution is unlimited. PA#

11

Propellant Mechanical Properties

- **Non-linear viscoelastic material**
- **Effective value for Young's modulus depends on:**
  - **Strain rate[1]**
  - **Temperature[1]**
- **Strain rate that propellant experiences during ignition is difficult to predict**
- **To determine propellant modulus value at ignition, high strain rate tensile test may be used[5]**

Prediction of Mass Flow Rate

- **Analytical calculation**
  - **Chamber pressure → burn rate → mass flow rate**
  - **No account for deformation or pressure drop**

- **Computational fluid dynamics (CFD)**
  - **Pressure calculation controls mass flow inlet**
  - **No account for deformation**

- **Fluid-structure interaction (FSI)**
  - **Couples CFD and finite element analysis (FEA)**
  - **Pressure calculation controls mass flow inlet**
  - **Deformation of structure due to pressure load**
  - **May be one-way or two-way[6]**

CFD for Solid Rocket Motors

- **ANSYS Fluent™ is one of the common codes[4]**
- **Combustion gas is complex**
  - **Burning aluminum droplets[1]**
  - **Non-homogeneous**
- **Common combustion gas simplifications for this type of analysis[4]**
  - **Single phase**
  - **Equivalent molecular weight**
  - **Homogeneous mixture**
  - **Chemically frozen**
  - **Calorically perfect**

FEA for Solid Rocket Motors

- **ABAQUS™ is one of the common codes[4,7]**
  - Linear elastic models
  - Non-linear viscoelastic models
  - Pressure loads
- **Elastic modulus[5]**
  - To model ignition, use data from high strain rate
  - To model storage conditions, use low strain rate data

Fluid-Structure Interaction Analysis

- ## One-way coupling[6]
  - ### Use CFD calculation to determine pressures
  - ### Apply pressures to structure for finite element analysis

- ## Two-way coupling[6]
  - ### Use CFD calculation to determine pressures
  - ### Apply pressures to structure for finite element analysis
  - ### Deformation of structure is applied to CFD mesh
  - ### Deformed CFD mesh calculates new pressures
  - ### Iterates until convergence criteria are met

Approved for public release; distribution is unlimited. PA#

16
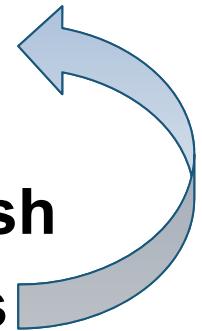
FSI Analysis

- **Manual FSI**
  - Analyst or computer interpolates pressure from CFD solution onto structure
  - FEA solution determines deformations
  - Analyst creates CFD mesh for deformed geometry
- **Automated FSI[8]**
  - Computer interpolates pressures from CFD, executes FEA, interpolates deformations onto CFD mesh, and executes CFD

Methodology

- **Design a motor that exaggerates the FSI effect**
- **Compare mass flow rate calculations**
  - **Analytical solution**
  - **CFD only**
  - **Manual fluid-structure interaction**
  - **Automated fluid-structure interaction**

$t_c=10$

$l_p=400$

$t_p=7.5$

A

$r_b=45.5$

B

$r_t=13$

units = mm

Axis of symmetry

$r_c=14$

$r_e=26$
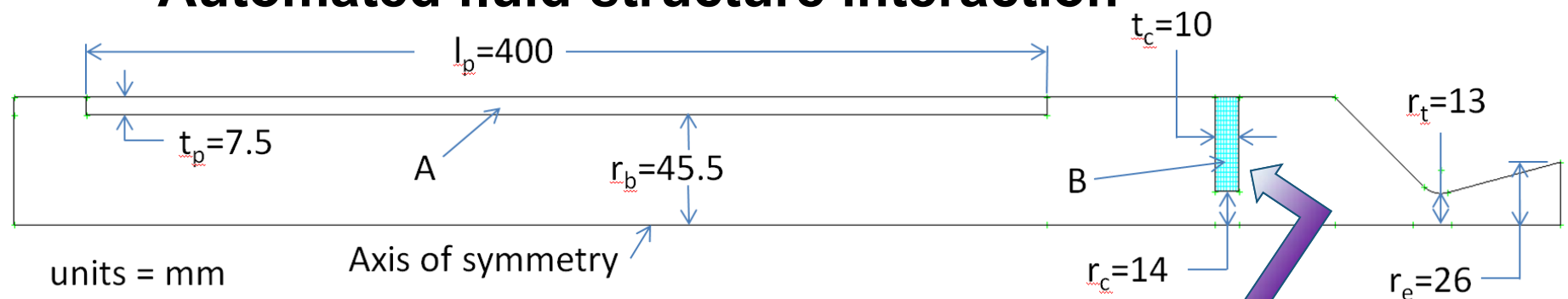
What effect does the deformation of the <u>flap</u> have on chamber pressure and mass flow rate?

Approved for public release; distribution is unlimited. PA#

18

Fluid and Structure Model Input Values

Propellant	Burn Rate Pressure Exponent, n	.34 (unitless)
	Reference Burn Rate, r_0	7.0 mm/s @ 6.89 MPa
	Young's Modulus, E	55.2 MPa
	Poisson's Ratio, v	0.499 (unitless)
	Density, ρ_s	1802 kg/m^3
Gas Properties	Gas Temperature	3,500 K
	Molecular Weight	29.56 kg/kmole
	Specific Heat, C_p	4113 J/K•kg
	Viscosity	1.034E-4 mP
	Characteristic Exhaust Velocity, $c*$	1,576 m/s

Approved for public release; distribution is unlimited. PA#

19

Analytical Solution

Propellant surface burn area, A_b

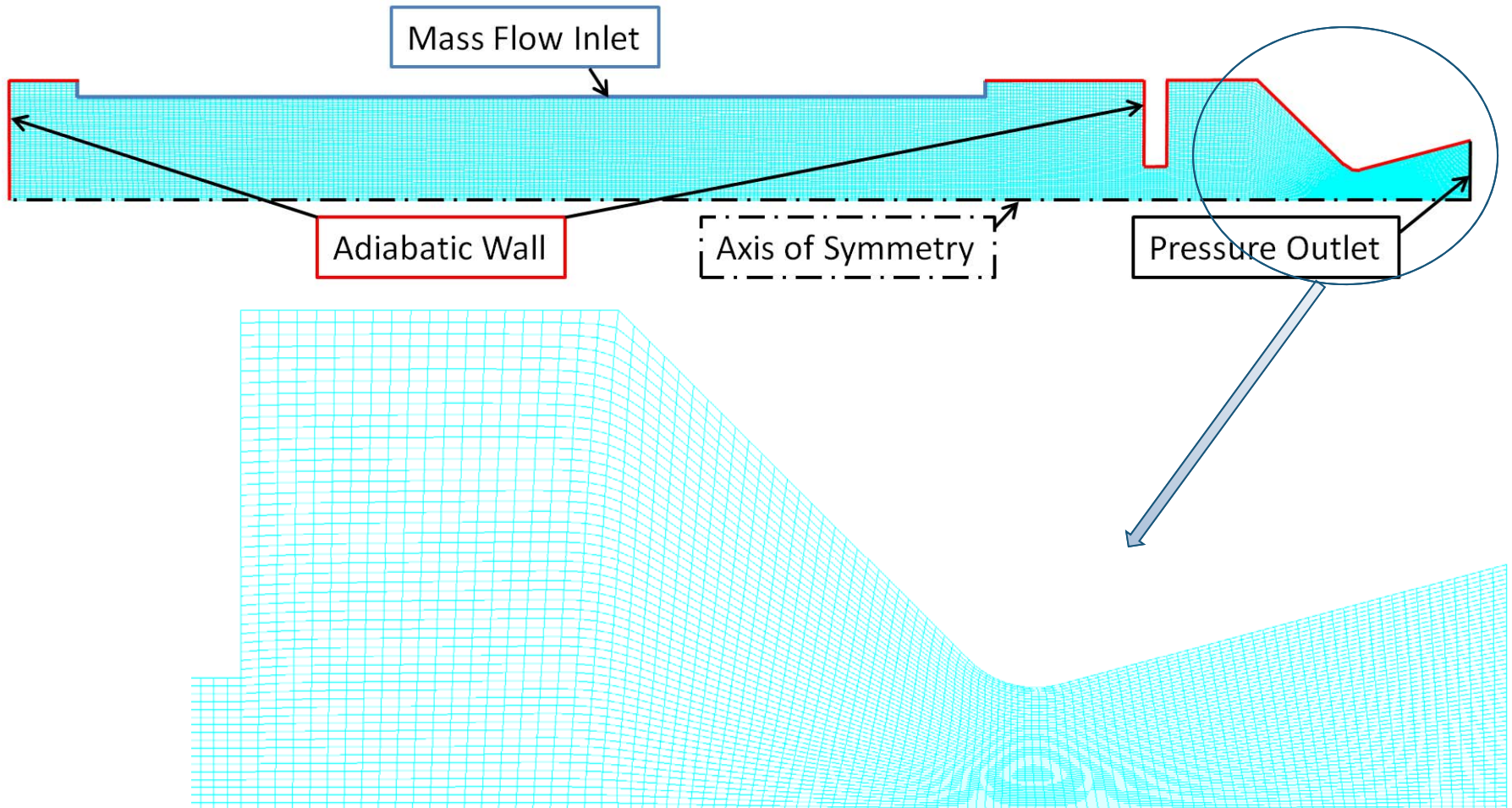| Motor Geometry	
Burn Surface Area, A_b	118,996 mm^2
Throat Area, A_t	531 mm^2

- **From previous equations**
  - **Chamber pressure = 3.55 Mpa (515 psia)**
  - **Mass flow rate = 1.198 kg/s**

CFD Solution - Setup

- ## ANSYS Fluent™ version 14.5

Mass Flow Inlet

Adiabatic Wall

Axis of Symmetry

Pressure Outlet
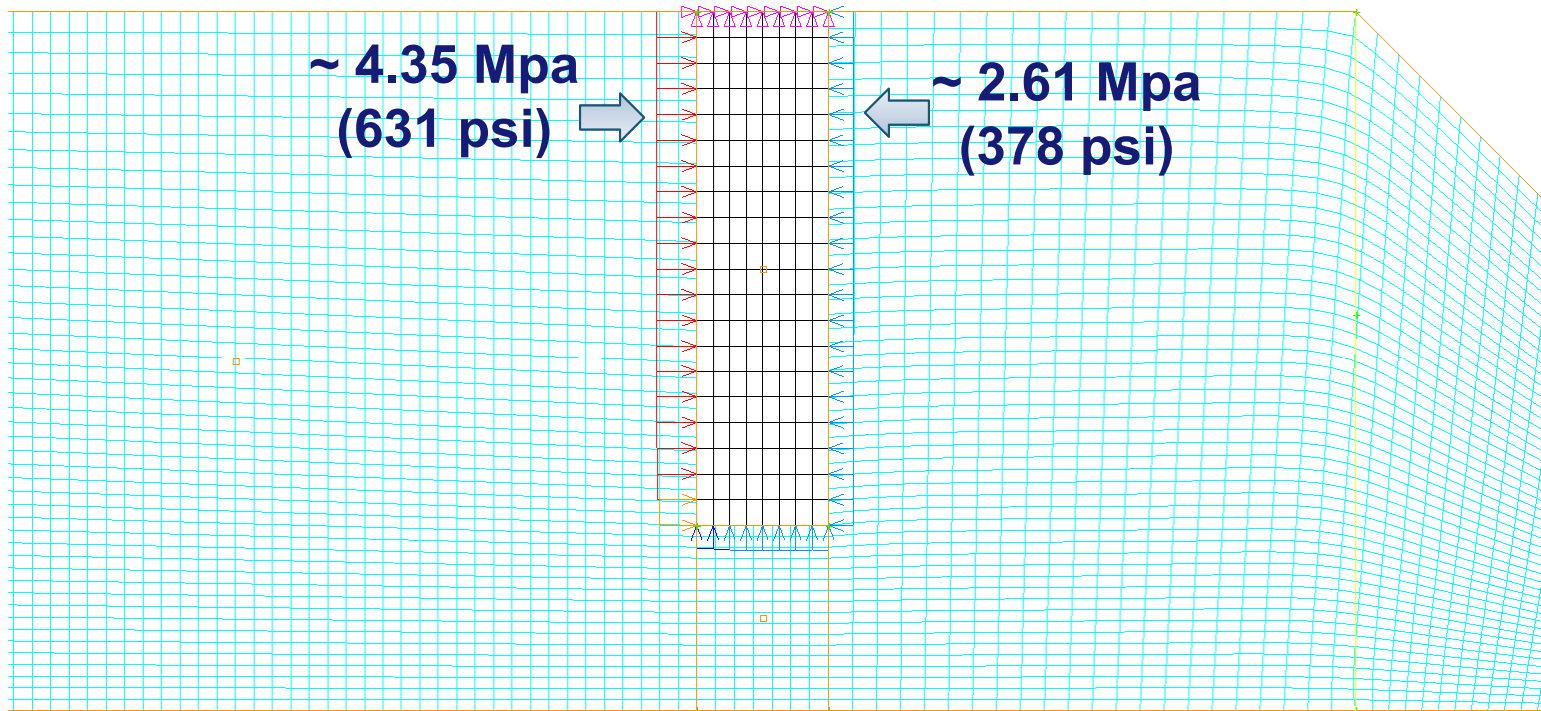
CFD Solution – Set-up (con't)

- **Viscous model: k-omega SST**
- **Mass flow inlet[4]**
  - **User Defined Function (UDF)**
  - **Determines mass flow amount for each element based on calculated local static pressure**
- **Convergence criteria**
  - **Residuals no longer decreasing**
  - **Mass conservation check between inlet and outlet**

Manual FSI – Initial CFD Solution

- **Utilize results of initial CFD solution**

- **Computer code FEM Builder™**

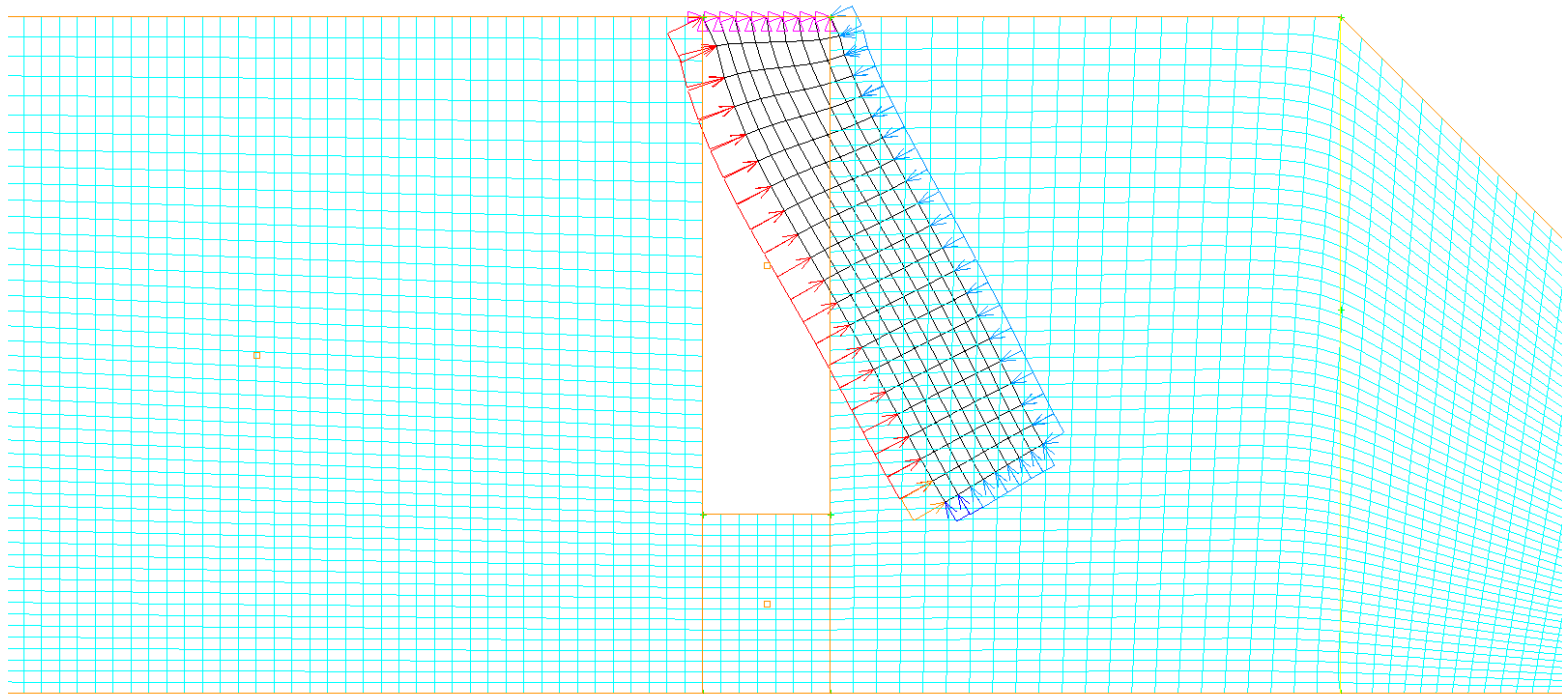 - **Interpolates pressure results onto structural model**

  - **Writes ABAQUS™ input file**

~ 4.35 Mpa
(631 psi)

~ 2.61 Mpa
(378 psi)

Approved for public release; distribution is unlimited. PA#

23

Manual FSI – Structural Deformation

- ## ABAQUS™ version 6.14
  - ### Static structural analysis
  - ### Convergence criteria (default)[7]
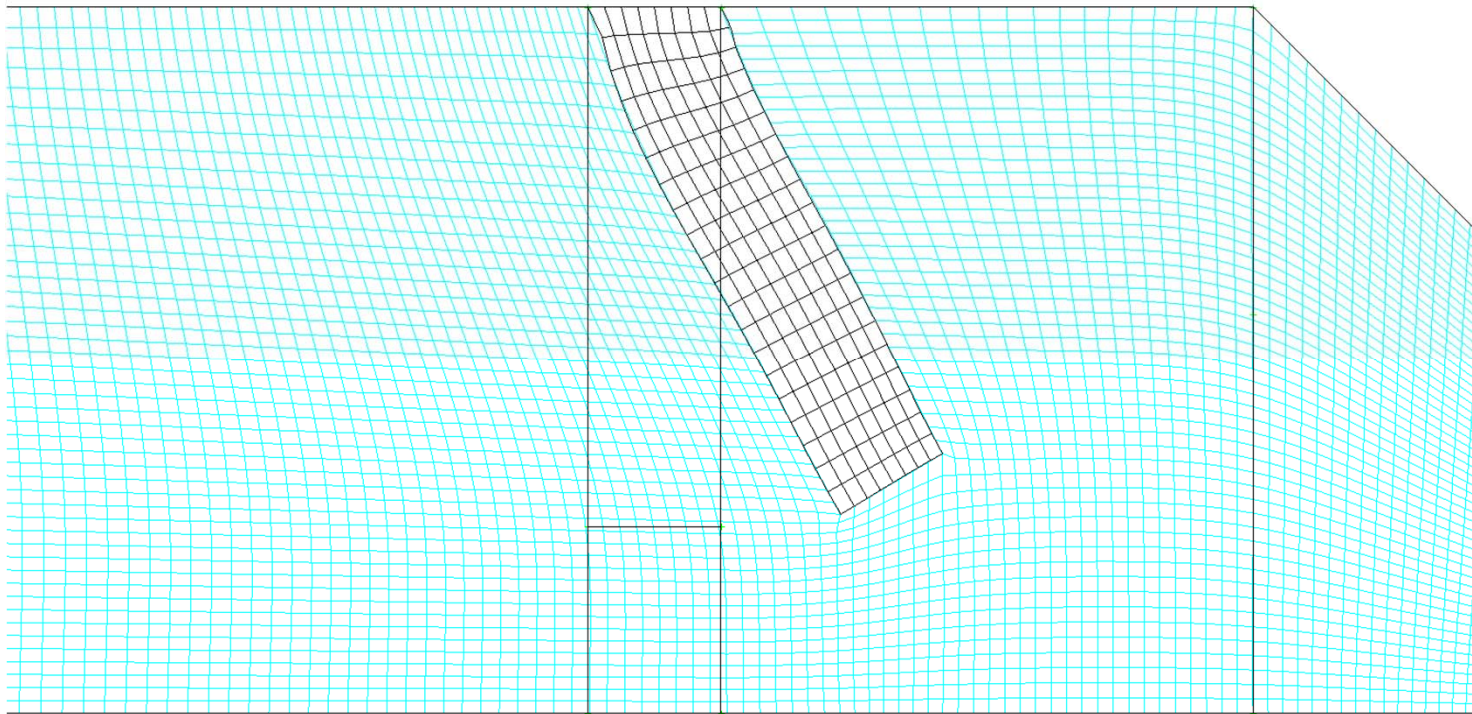   - #### Ratio of largest residual to average flux norm = 5E-3

Manual FSI – Fluid Mesh Deformation

- **Deformed structure traced in FEM Builder™**
- **Number of fluid elements retained**
- **Deformed CFD mesh solved with Fluent™**

Approved for public release; distribution is unlimited. PA#

25

Automated FSI

- **Utilize results of initial CFD solution**

- **FEM Builder™,[8]**

  - **Interpolates pressure onto structure**

  - **Writes and executes ABAQUS™ input file**

  - **Interpolates displacement of structural nodes on interface onto fluid nodes on interface**

  - **Deforms fluid mesh**

  - **Writes and executes Fluent™ case file**

  - **Iterates until convergence criteria are met**

    - **Maximum static pressure: 0.1% change**
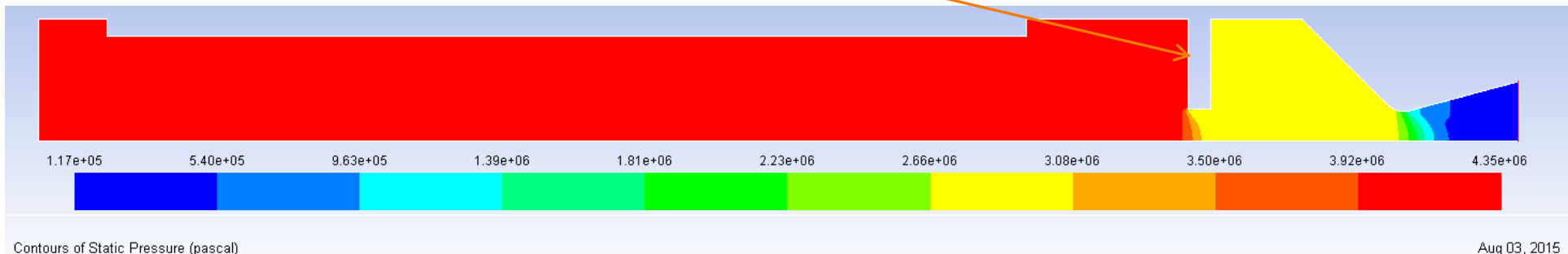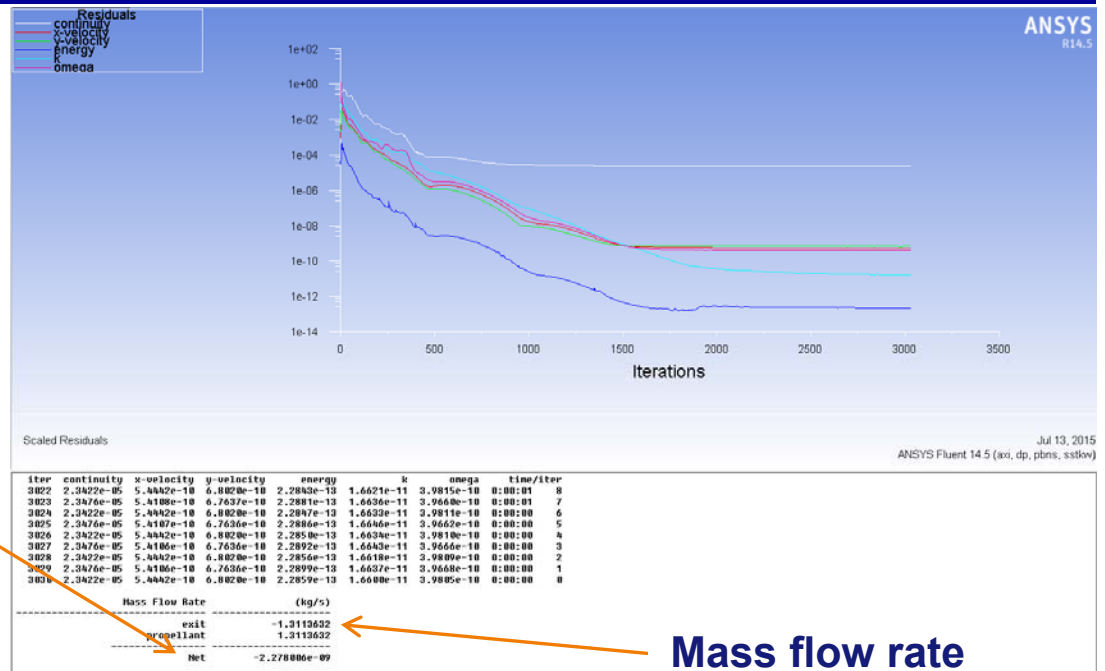
    - **Maximum displacement: 0.1% change**

Approved for public release; distribution is unlimited. PA#

26

CFD Solution - Results

- ## Residuals
  - ## 10E-5 to 10E-13
  - ## No longer changing

- ## Mass conservation
  - ## Error < 2E-7%

- ## Large pressure drop across flap

Mass flow rate calculated by Fluent™

Manual FSI Solution - Results

- ## Residuals
  - ## 1E-10 to 1E-15
  - ## No longer changing

- ## Mass conservation
 - ## Error < 9E-14%

- ## 1 Iteration FSI

Scaled Residuals

Jul 15, 2015
ANSYS Fluent 14.5 (axi, dp, pbns, sstkw)

1.06e+05 4.24e+05 7.42e+05 1.06e+06 1.38e+06 1.70e+06 2.01e+06 2.33e+06 2.65e+06 2.97e+06 3.29e+06 3.60e+06 3.92e+06

Contours of Static Pressure (pascal)

Aug 03, 2015
ANSYS Fluent 14.5 (axi, dp, pbns, sstkw)
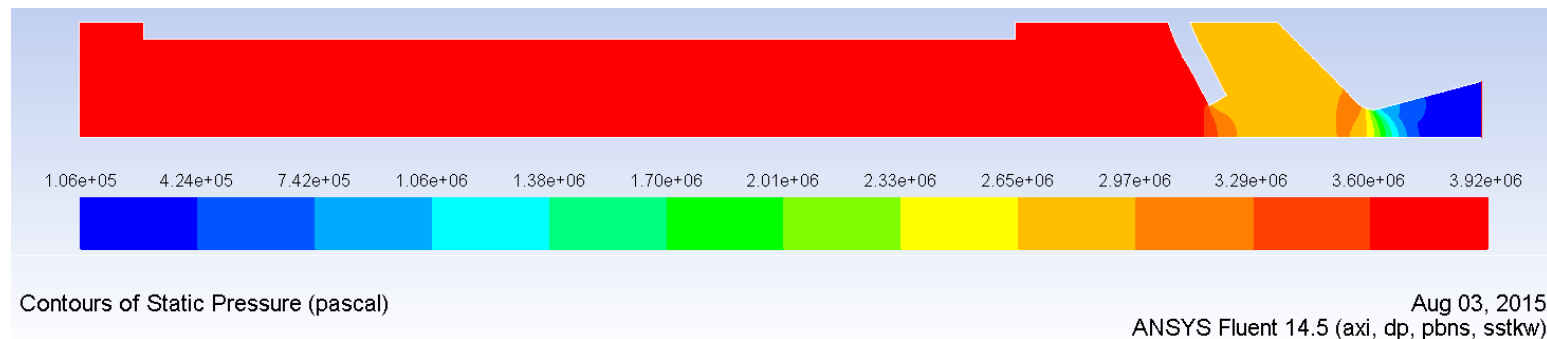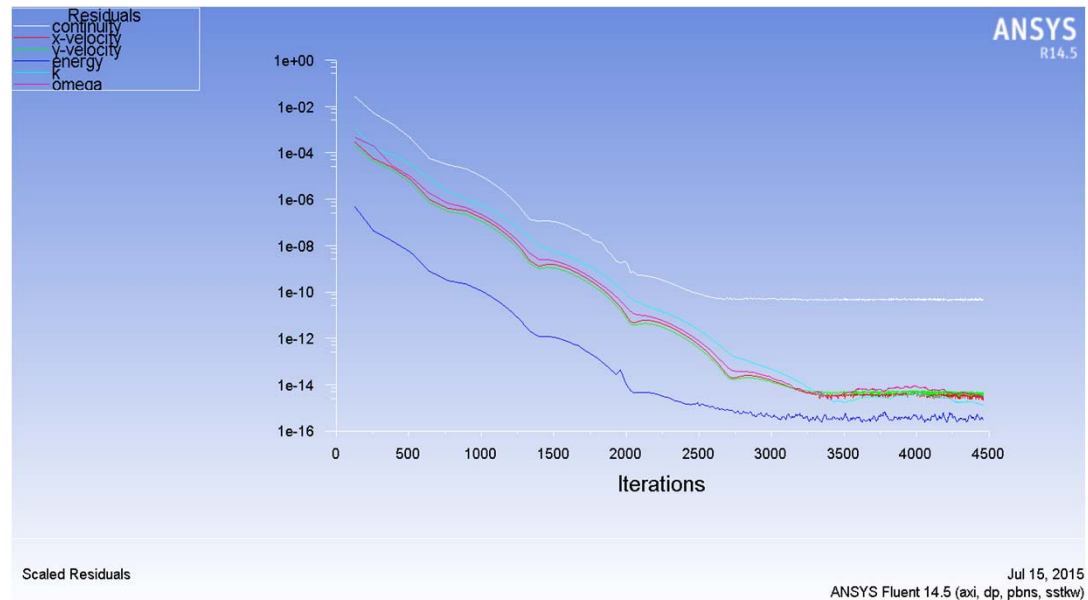
```
          Mass Flow Rate          (kg/s)
------------------------    --------------------
               exit              -1.2493766
          propellant              1.2493766
------------------------    --------------------
                Net            1.110223e-15
```

Automated FSI Solution - Results

- **1st deformed CFD solution failed due to excessive deformation**
  - **Automated CFD deformation resulted in highly skewed elements**
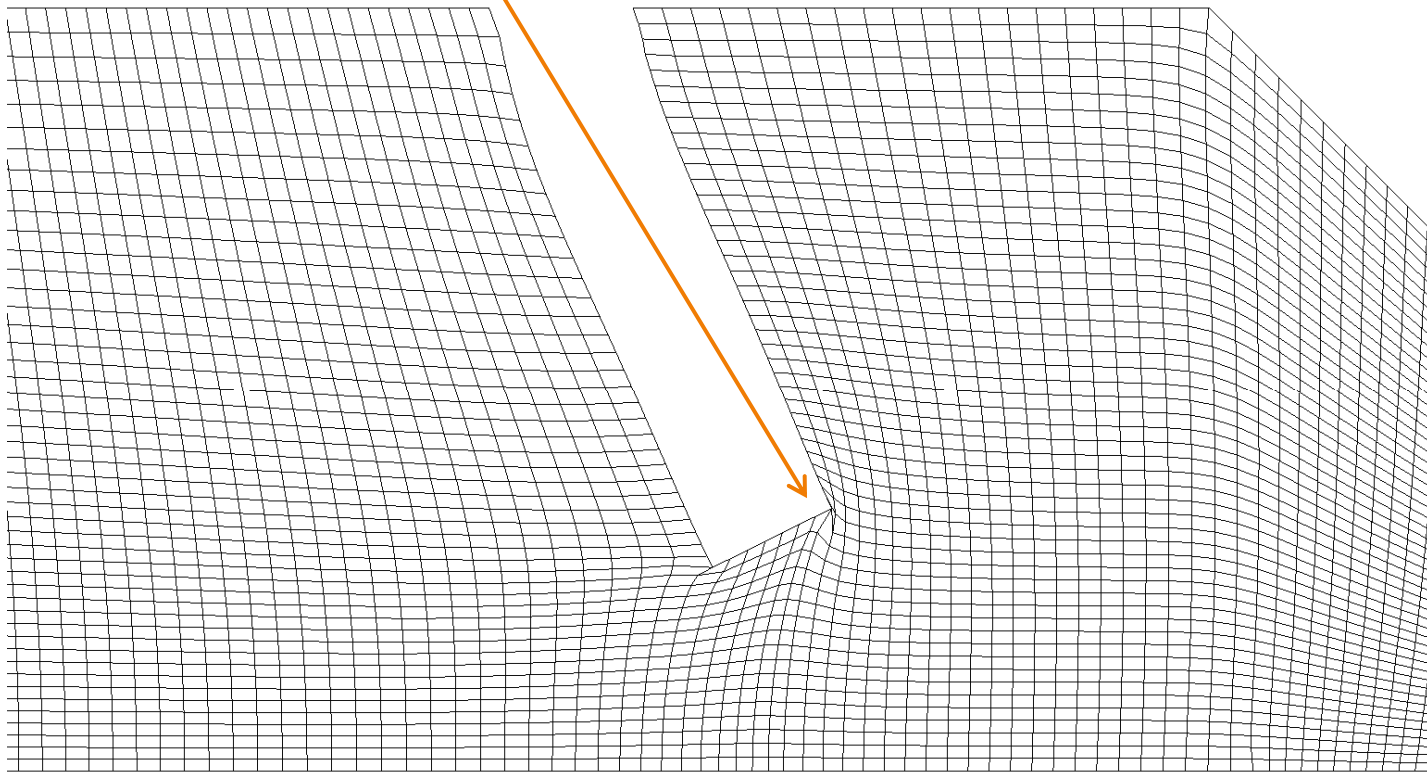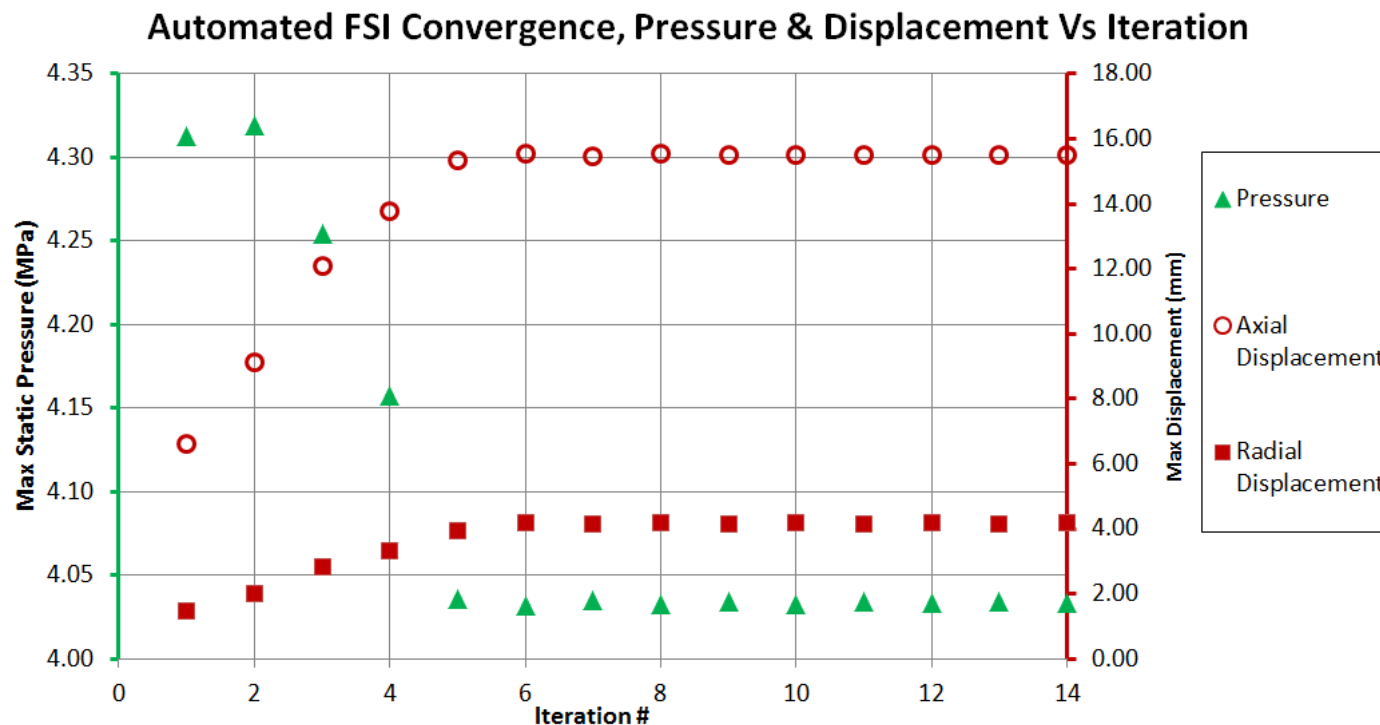
Automated FSI Solution – Results Pressure Loading Factor

- **Pressure result is reduced before application as structure pressure load**

- **Ramp up over 5 iterations (0.2, 0.4, 0.6, 0.8, 1.0)**
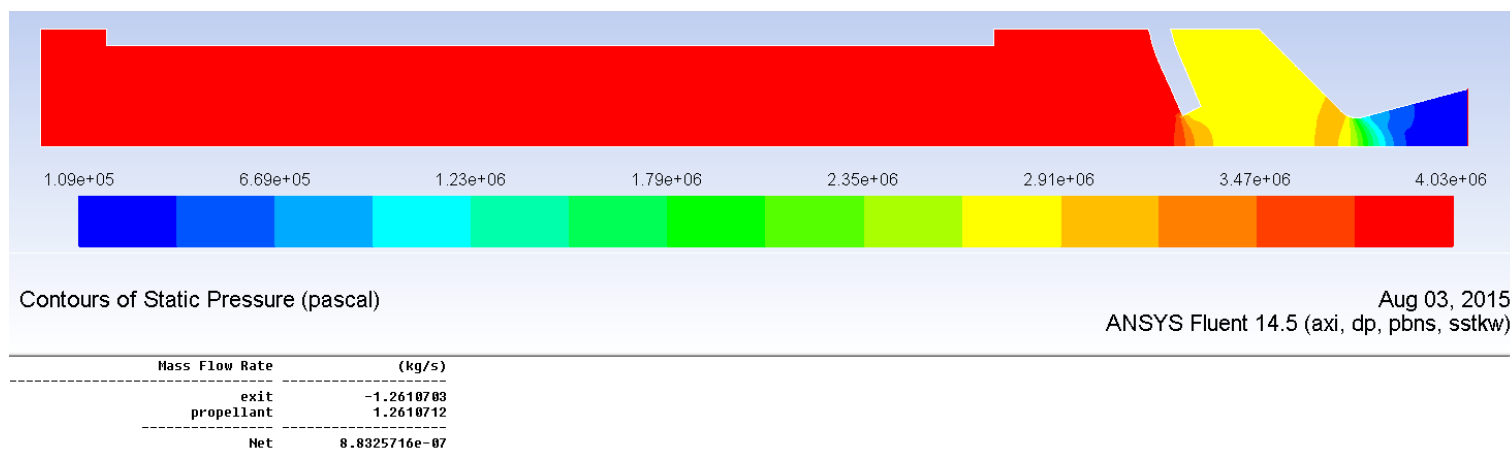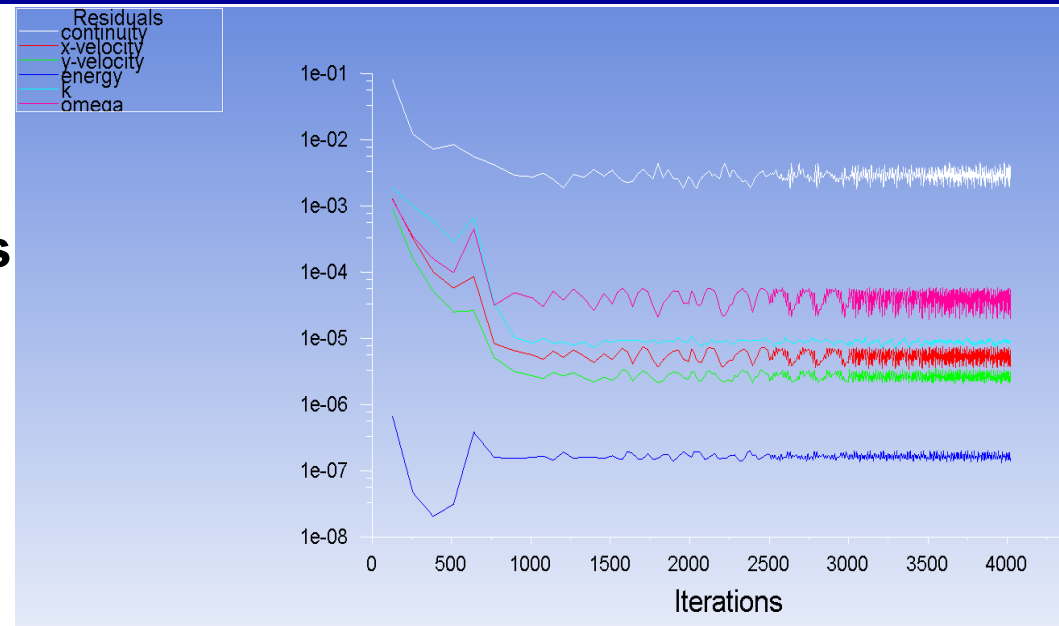
- **Prevents "overshoot" of deformation**

Automated FSI Convergence, Pressure & Displacement Vs Iteration

Automated FSI Solution - Results

- ## Residuals
  - ## 1E-2 to 1E-6
    - **Not as low as previous**
  - ## No longer changing
    - **"Buzzing"**

- ## Mass conservation
  - ## Error ~ 7E-5%

Residuals
continuity
x-velocity
y-velocity
energy
k
omega

Contours of Static Pressure (pascal)

Aug 03, 2015
ANSYS Fluent 14.5 (axi, dp, pbns, sstkw)

```
          Mass Flow Rate        (kg/s)
     ----------------    ------------------
              exit          -1.2610703
          propellant         1.2610712
     ----------------    ------------------
               Net         8.8325716e-07
```
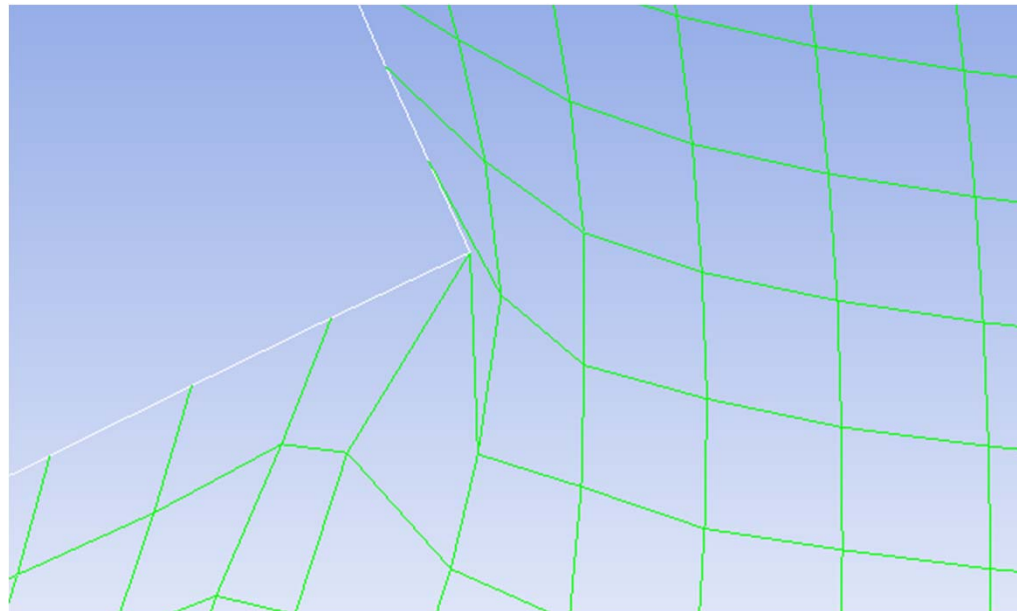
Automated FSI Solution – Results
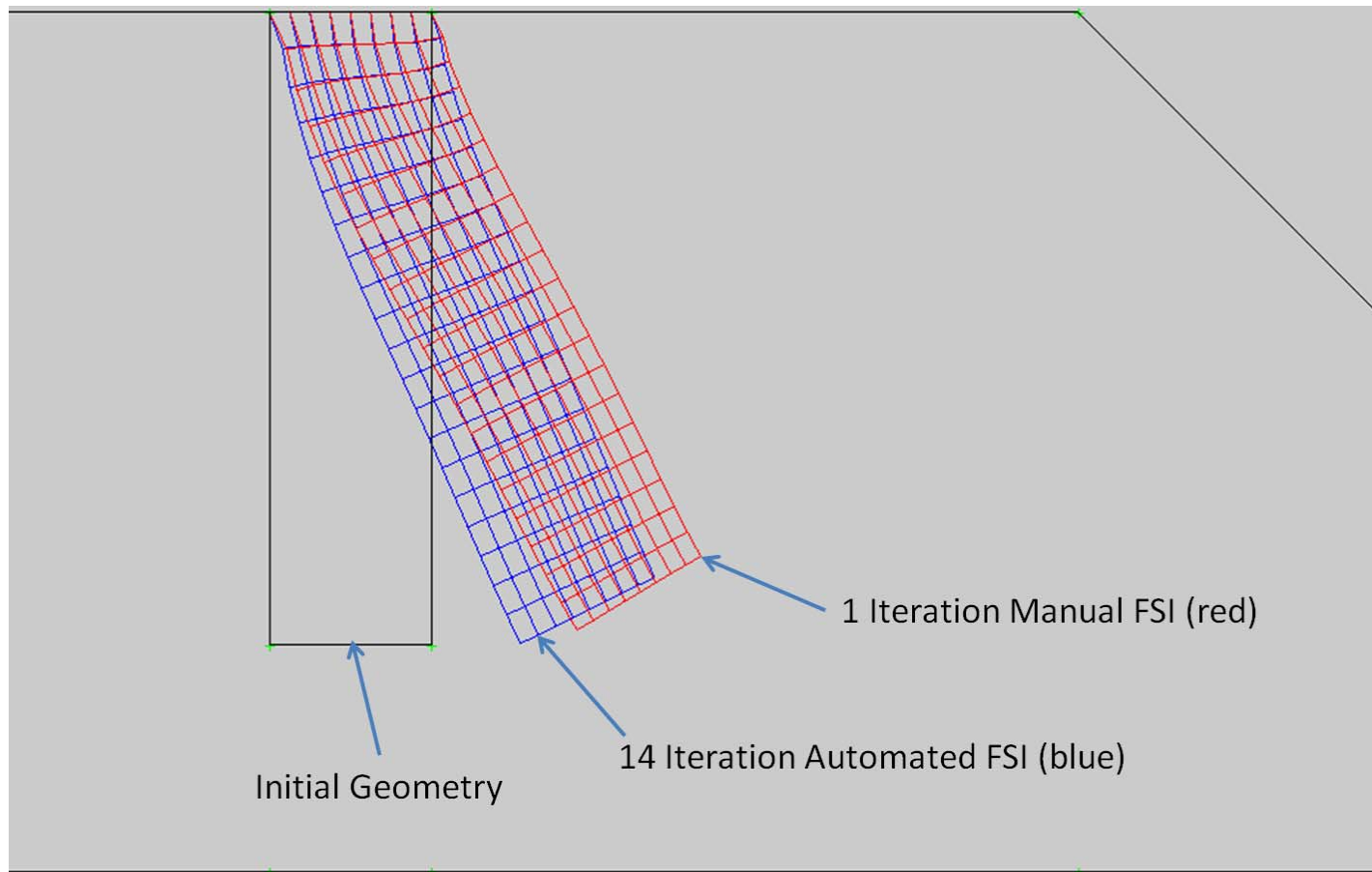## CFD Deformation Issue

- **Results are similar to 1st deformed CFD solution failure, except not as severe**

- **CFD mesh is deformed by structural solver**
  - **No ability to relocate and smooth inner nodes**

FSI Deformation Comparison

1 Iteration Manual FSI (red)

14 Iteration Automated FSI (blue)

Initial Geometry

Pressure and Mass Flow Rate Results

- **Head-end pressure calculated by Fluent™**

- **Mass flow rate calculated by Fluent™**

- **Mass flow rate also calculated by:**

$$\dot{m} = \rho A_b r$$

where,

$$r = aP^n$$
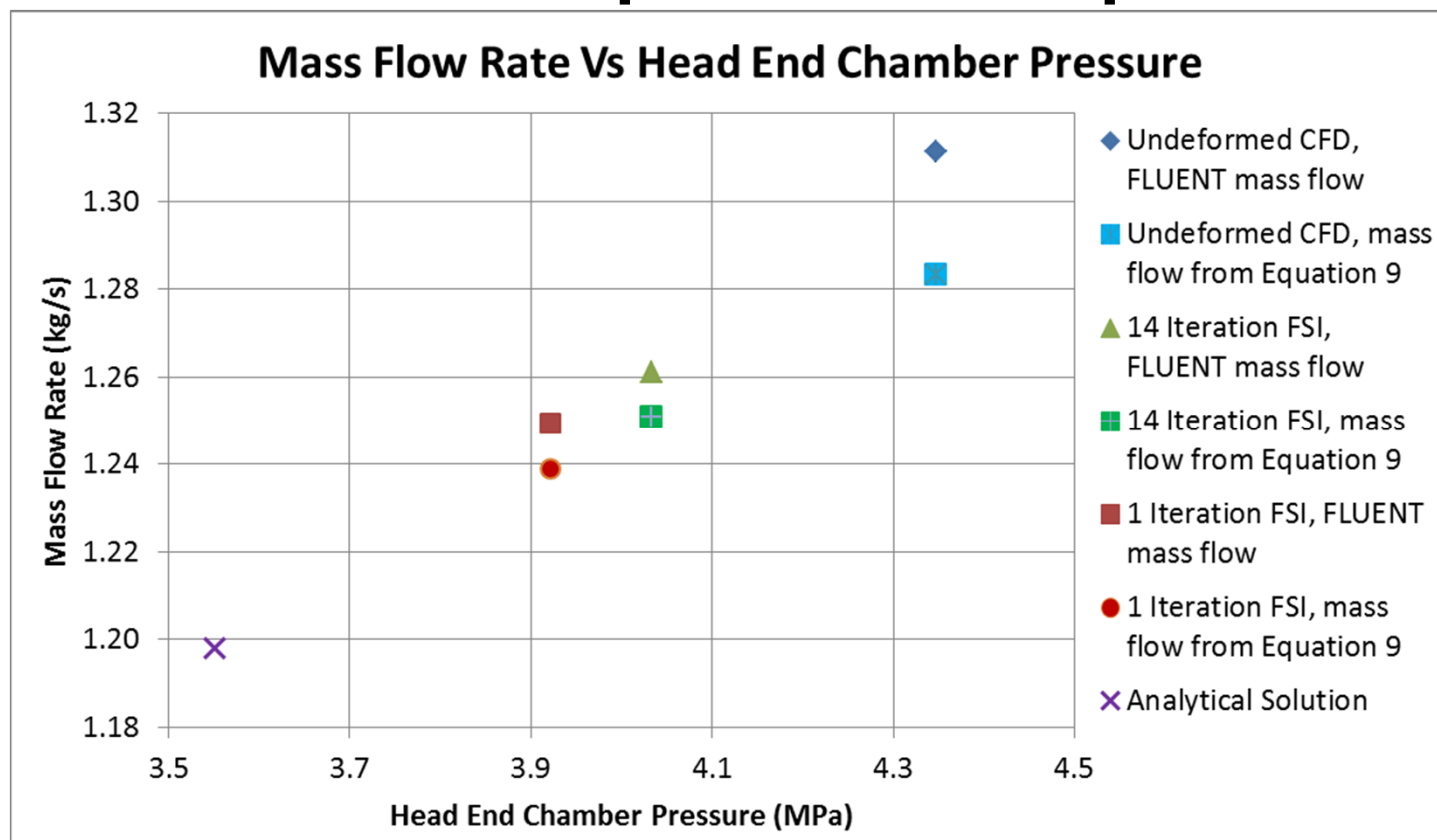
and P is the head-end pressure.

- **Pressure along propellant surface did not vary from calculated head-end pressure**

Pressure and Mass Flow Rate Results (con't)

- **No explanation for difference in mass flow rates from Fluent™ and Equation 9 in report**

Equation 9: $\dot{m} = \rho_s A_b r_i$

Conclusion

- **Mass flow rate is affected by structural deformation within a solid rocket motor**

- **Manual FSI analysis allows greater control over fluid mesh deformation**

- **Automated two-way coupling of fluid and structural models provides more accurate assessment of solid rocket motor internal ballistics**

Approved for public release; distribution is unlimited. PA#

36

References

- 1 Sutton, George P. "Rocket Propulsion Elements" Fourth Edition, John Wiley & Sons, New York, 1976

- 2 NASA website **https://www.grc.nasa.gov/www/K-12/airplane/rockth.html** accessed 21 July 2015

- 3 Murdock, John W.; Johnston, William A. "Flow-Structural Interaction in Solid Rocket Motors" NATO RTO-EN-023, Belgium, 2002

- 4 Rex, Brian W.; Wang, Qunzhen; Isaac, Daron, "An Automated Fluid-Structural Interaction Analysis of a Large Segmented Solid Rocket Motor", AIAA-2003-4507, 39th AIAA/ASME/SAE/ASEE Joint Propulsion Conference & Exhibit, July 20-23, 2003, Huntsville,   AL

- 5 Manpa Report NR 473 (82), Propellant Surveillance Report ANB-3066 Propellant, Propellant Analysis Laboratory, Hill Air Force Base, UT, August 1982

- 6 Benra, Friedrich-Karl; Dohmen, Hans Josef; Pei, Ji; et.al. "A Comparison of One-Way and   Two-Way Coupling Methods for Numerical Analysis of Fluid-Structure Interactions," Journal of Applied Mathematics, Volume 2011, Article ID 853560, 2011

- 7 Abaqus Version 6.14 Analysis User's Manual, Volume II, Part III

- 8 Isaac, Daron; Iverson, Michael, "Automated Fluid-Structure Interaction Analysis", ADA416478 Technical Reports **www.dtic.mil** accessed 15 July, 2015

Approved for public release; distribution is unlimited. PA#

37